288

SPACE CHARGE MEASUREMENT IN DIELECTRICS AND INSULATING MATERIALS

< PEA, PWP (PIPWP & LIPP) and TSM methods >

Task Force
D1.12.01

February 2006

SPACE CHARGE MEASUREMENT
IN DIELECTRICS AND INSULATING MATERIALS

< PEA, PWP (PIPWP & LIPP) and TSM methods >

Task Force

D1.12.01

T. Takada, J. Holboell, A. Toureille, J. Densley,
N. Hampton, J. Castellon, R. Hegerberg, M. Henriksen,
G.C. Montanari, M. Nagao, P. Morshuis

Space Charge Measurement in Dielectrics and Insulating Materials

Guide for Space Charge Measurement in Dielectrics and Insulating Materials

Abstract

Over the last few years there has been considerable interest in the measurement of the space charge distribution within dielectrics under AC and DC stress conditions. This interest has led to the development of a number of widely used techniques that enable to estimate the position and magnitude of trap charge within the dielectric. This paper provides a guide of the pressure methods and the thermal step method for space charge measurement in dielectrics and insulating materials.

1. Introduction

Task force 3 of Study Committee, CIGRE, TF 15-03, has published a review of the commonly used measuring methods of space charge distribution within dielectric materials [1]. The review contains a more detailed list of references than this report. In 1980s, a Piezoelectric Induced Pressure Wave Propagation (PIPWP) method [2] and a Laser Induced Pressure Propagation (LIPP) method [3, 4] were used to generate a narrow pressure wave, which could be used as a stimulating source to deform the sample uniformly. By this method, a space charge profile could be obtained by detecting the short circuit current. For the first time, very narrow duration pressure waves were used in the direct measurement of space charge distribution in solid dielectrics. In the beginning, this method was mainly used in "electret" research, with a very thin sample thickness less than about 100μm. In the 1980s, the methods were applied to insulation materials, which helped in the improvement of electric insulating materials. The Pulsed Electro-Acoustic Method (PEA) was also developed [5, 6] in 1980s. This method is based on the effect of an electric field induced acoustic wave on space charge. By detecting the acoustic wave generated by the space charge, one could know the space charge distribution in the dielectric. The PWP methods (PIPWP, LIPP) and PEA have been applied to various material specimens [7, 8], various conditions of AC voltage [9], gamma radiation [10], and power cables [11, 12].

In the case of the Thermal Step Method (TSM) [13-15], the stimulus which allows the measurement of the electric charge is a heat wave. The propagation of the thermal wave across the dielectric generates a temporary local disequilibrium of the space charge. This disequilibrium is reflected at the electrodes by a variation of the influence charges, which allows determining the distribution of the electric field and charge density in the sample. Since 1986, the TSM has been applied to various material specimens [16] and industrial components; power cables [17, 18], capacitors [19], printed circuit boards [20], and stator windings [21].

Several other methods for space charge measurement as shown in Table 1 were developed in this period. Information on the experimental setup and the discussion of the measurement methods

were exchanged at many international conferences. Today, these methods are actively used to measure space charge distribution directly, quantitatively, and non-destructively.

Table 1: Measurement methods of space charge distribution

Measurement Method	Excitation method	Measurement signal	References for principle	References for applications
PIPWP	Nanosecond pressure pulse	Nanosecond electric signal	[2], [22]	[8],
LIPP	Nanosecond pressure pulse	Nanosecond electric signal	[3], [4]	[11]
PEA	Nanosecond electric pulse	Nanosecond Pressure signal	[5], [6]	[7], [9], [10], [12]
TSM	Thermal step	Electric current	[13], [14], [15]	[16], [17], [18], [19], [20], [21]
TPM	Thermal pulse	Electric signal	[23]	
LIM	Modified thermal pulse	Electric current	[24]	
EBM	Electron beam irradiation	Electric current	[25]	

TPM: (Thermal Pulse Method), LIM: (Laser Intensity Modulation), EBM: (Electron Beam Method)

This technical report is limited to the widely used methods of PIPWP, LIPP, PEA and TSM. The four methods will be described in the following chapters (see §2, 3 and 4 for the pressure methods and §5, 6 and 7 for the Thermal Step Method).

2. PEA and PWP Space Charge Measurement Equipment and Results

2.1 Pulsed Electro Acoustic (PEA) method

The principle of the PEA method is shown in Figure 1. Consider a sheet sample with thickness d and space charge distribution ρ(z). A pulsed electric field e(t) is externally applied to the sample and induces a perturbation electric force on each charge. This force causes the charge to move slightly in its position. This movement launches an acoustic pressure wave p(t) as shown in Equation (1) that is proportional to the charge distribution ρ(z) in the sample. A piezoelectric transducer is used to detect the acoustic wave and transform the acoustic wave into an electric charge signal q(t) as shown in Equation (2). These equations were obtained under condition of acoustic matching between the test sample and the backing material of the high voltage electrode. Details of PEA method are published in elsewhere [22].

$$p(t) = \frac{Z_{Al}}{Z_{sa} + Z_{Al}} \times \left[\sigma(0)\, e(t) + u_{sa} \int_{-\infty}^{+\infty} \rho(\tau)\, e_p(t-\tau) d\tau + \sigma(d)\, e\left(t - \frac{d}{u_{sa}}\right) \right] \quad (1)$$

$$q(t) = \frac{2Z_p}{Z_{Al} + Z_p} \frac{u_p}{b} \int_{-\infty}^{+\infty} h(\tau) p(t-\tau) d\tau \quad (2)$$

where Z_{Al} is the acoustic impedance of the ground electrode, Z_{sa} is the acoustic impedance of the sample, Z_p is the acoustic impedance of the transducer, u_{sa} is the acoustic velocity in the sample, u_p is the acoustic velocity in the transducer of thickness b, σ(0) is the surface charge on the ground electrode, and σ(d) is the surface charge on the high voltage electrode.

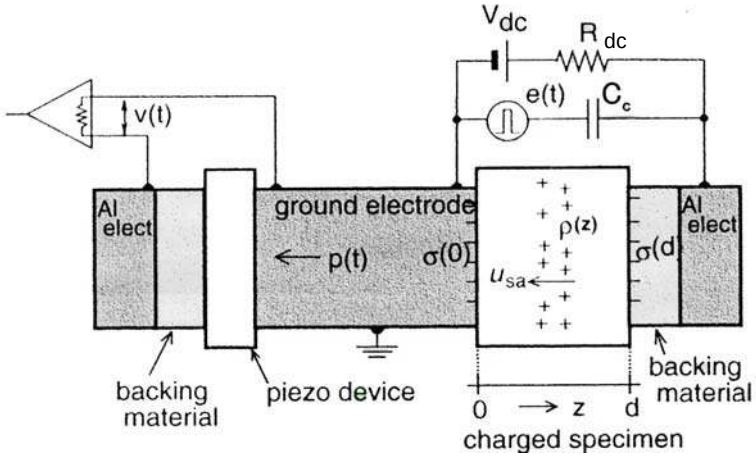

Figure 1: PEA space charge measurement system.

2.2 Pressure Wave Propagation (PWP) method

The principle of a PWP method can be seen in Figure 2, showing the PIPWP method, where the acoustic wave is generated by a piezoelectric device. In case of the LIPP method, the acoustic wave is generated by laser pulse absorption on a target material. The acoustic wave p(t) in Equation (3) acts as a charge probe. The charge moves as the acoustic wave propagates through it. This movement causes a change of the surface charges on the electrodes. The time signal of the displacement current

i(t) indicates the charge distribution in the sample as shown Equation (4). By measuring the displacement current between the electrodes, the charge distribution is obtained. These equations were also obtained assuming acoustic matching between the test sample and the backing material of the high voltage electrode. Details of PWP method are published elsewhere [2-4].

$$p(t) = \frac{Z_{Al}}{Z_p + Z_{Al}} \frac{u_p}{a} \int_{-\infty}^{+\infty} g(\tau) e(t-\tau) d\tau \tag{3}$$

$$i(t) = \frac{2Z_{sa}}{Z_{Al} + Z_{sa}} \frac{A(f)}{Y} \frac{u_{sa}}{d} \left[\sigma(0)p(t) + u_{sa} \int_{-\infty}^{+\infty} \rho(\tau)p(t-\tau)d\tau + \sigma(d)p(t-\frac{d}{u_{sa}}) \right] \tag{4}$$

where a is the thickness of the transducer and the remaining terms are the same as those in Equations (1) and (2).

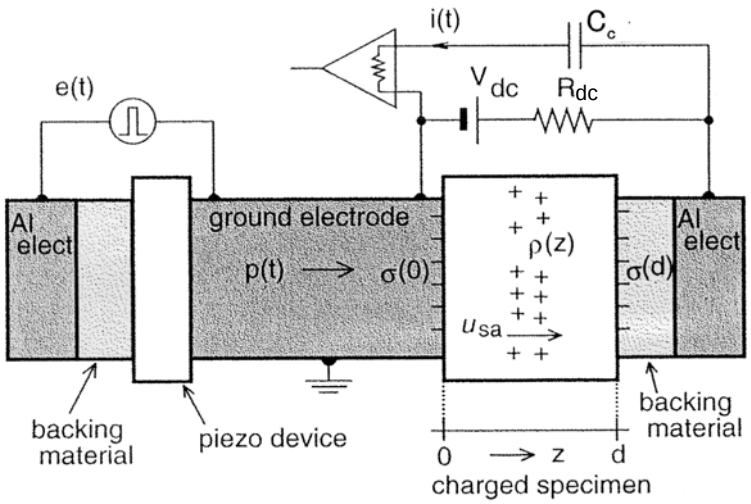

Figure 2: PWP space charge measurement system(here PIPWP).

2.3 Space Charge, Electric Field and Potential Distribution Results

Two PMMA samples (0.5 mm) are measured using both PEA and PWP methods for comparison. Sample A contains no space charge, while sample B is irradiated by an electron beam (200 kV and 1.0 nA/cm^2 for 3 hours) to accumulate a space charge distribution.

For sample A, surface charges are induced by a HVDC (V_{dc}=2 kV) applied to the sample. The results using PEA and PWP methods are shown in Figures 3 and 4 respectively. In principle, the surface charge densities σ(0) and σ(d) should be a delta function if expressed in coordinates of volume space charge density. However, due to the finite resolution of the detecting device and the finite width of the generated pulse, it is not possible to obtain this ideal result. Consequently, the induced surface charges are expressed as a negative and positive peaks as shown in Figures 3 (a) and 4 (a). The widths of the peaks reflect the resolution of the measurement system. The narrower the width, the higher the resolution. The full width at half height for both systems is about 16 μm indicating that the resolutions of both the PEA and PWP systems are almost the same.

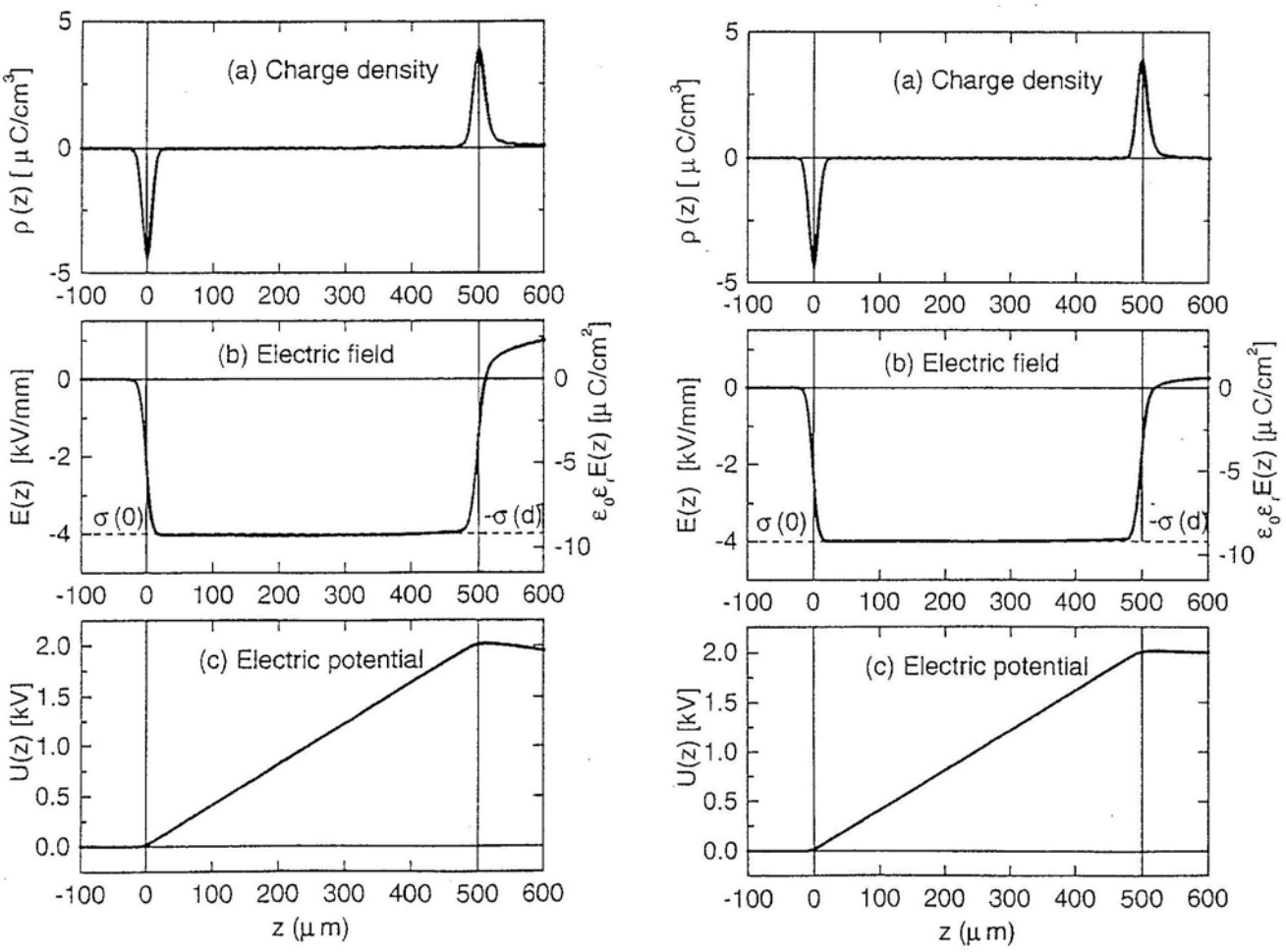

Figure 3 & 4: Experimental results of sample A using PEA (left) and the PIPWP method (right)

The distribution of the electric field E(z) along the z direction is calculated by integrating $\rho(z)/\varepsilon_r\varepsilon_0$. The distribution of the electric potential V(z) is obtained from the integration of E(z). The results are shown in Figures 3 (b) and (c) and Figures 4 (b) and (c) for the PEA and PWP methods respectively. As expected, inside the sample, the electric field E(z) is almost a horizontal line at –4 kV/mm and the potential V(z) varies from 0 to 2 kV linearly for both methods. The surface charge density can be obtained from the extension of the straight line of E(z) to the right axis $\varepsilon_r\varepsilon_0$ E(z=d) in Figures 3 (b) and 4 (b). The calculated surface charge density at z=0 and z=d(=0.5 mm) are σ(o) =-8.1 nC/cm2 and σ(d) =-8.1 nC/cm2 for both the PEA and PWP methods. In theory, the electric field should approach 0 when z is larger than the thickness of the sample. However, due to the mismatch in the acoustic impedance between the sample and the backing material of the electrode, the detected signal are distorted outside the sample. Consequently, E(z) does not approach 0 when z is larger than the thickness of the sample as shown in Figures 3 (b) and 4 (b).

The short-circuited space charge distribution of sample B, which is irradiated by an electron beam, is shown in Figures 5 (a) and 6 (a) for the PEA and PWP methods respectively. The results from both methods are almost the same. A negative peak at z=160 μm is due to a concentration of irradiated electrons. The maximum penetration depth of the irradiated electrons is about 400 μm.

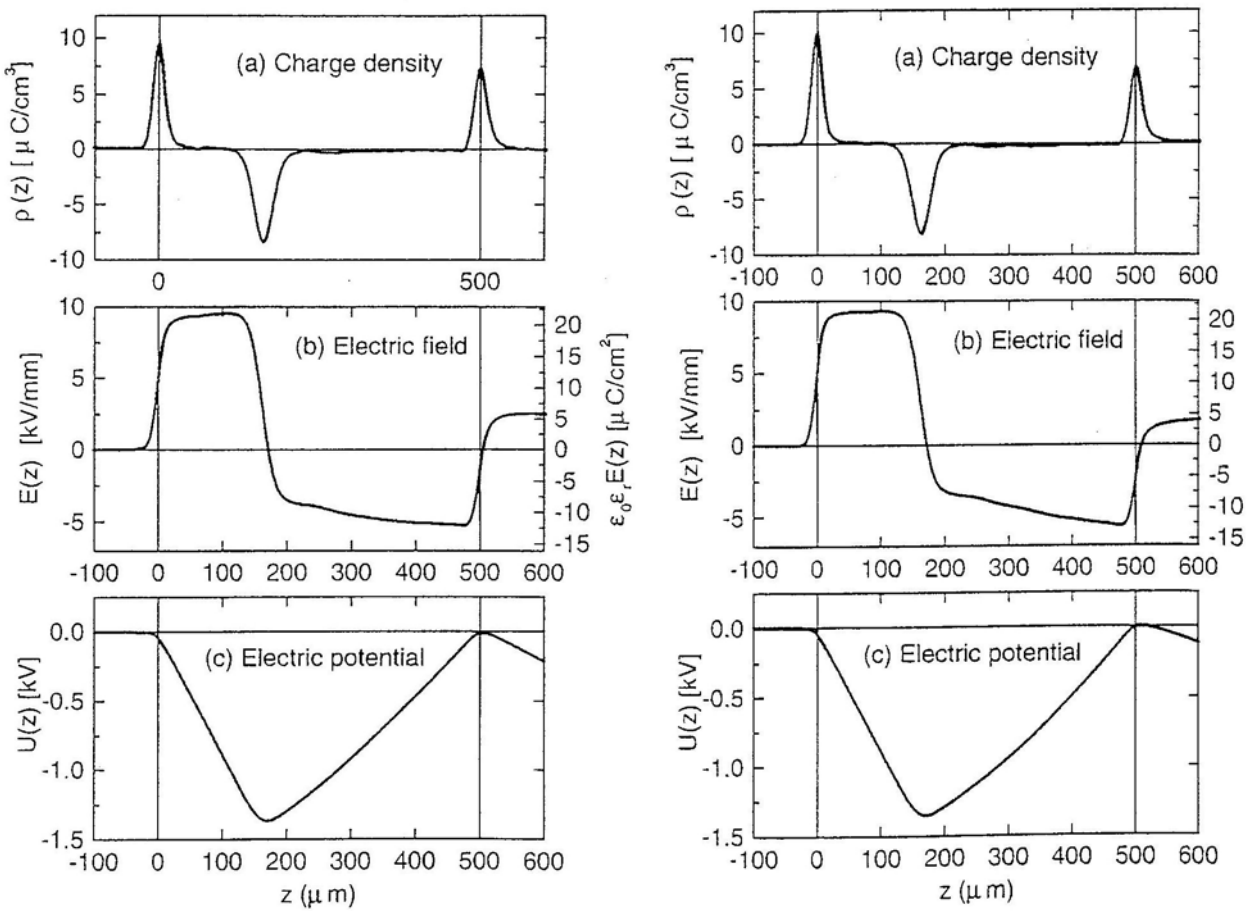

Figure 5 & 6: Experimental results of sample B using the PEA (left) and PIPWP method (right)

Due to induced charges, two peaks are found at z=0 and 500 μm. The distribution of electric field E(z) and potential V(z) are shown in Figures 5 (b) and (c) and Figures 6 (b) and (c) for PEA and PWP methods respectively. The electric field is zero at z=190 μm in the sample. The potential distribution in the sample looks like an inverted triangle as illustrated in Figure 5 (c) and Figure 6 (c). On both surface of the sample, the potential approaches zero as expected. The peak of the inverted triangle is located at z=190 μm, corresponding to the position where E(z) is zero. As already mentioned, the pulse acoustic techniques of both PEA and PWP methods can evaluate the accumulated space charge distribution ρ(z), and also the electric field distribution E(z) and potential distribution V(z) in insulating materials.

3. Standard Measurement Conditions for Pressure Methods

In general the measurement equipment should have the required accuracy and reproducibility of data. In this section the standardized measurement conditions are mentioned to measure the space charge distribution in solid dielectrics.

3.1 Sample Thickness and Pulse Duration

The space resolution of space charge distribution is mainly determined by the duration ΔT_p of the pulse electric field for the PEA method or the duration ΔT_a of the acoustic pulse for the PWP method. The conditions for the selection of the optimum duration are now described.

(1) Definition of Relative Space Resolution

As shown in Figure 7, a rectangular space charge region in the sample is assumed. Due to this space charge, surface charges σ(0) and σ(d) are induced on the surfaces of the electrodes. The signal waveform is also shown in Figure 7 according to the relative spatial resolution (a)Δz/d=1%, (b) 2%, (c) 4%, and (d) 8% respectively.

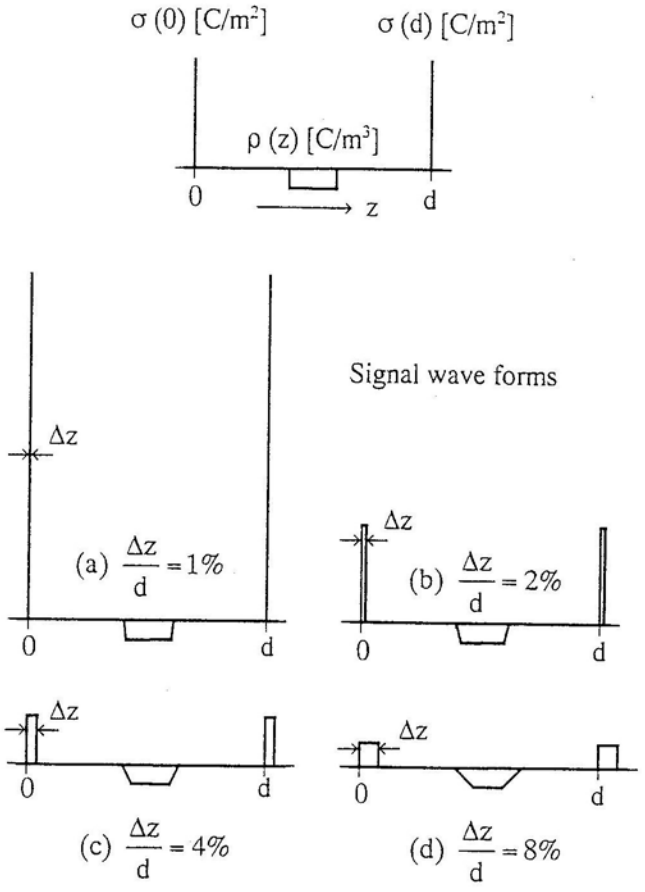

Figure 7: Relationship between signal waveform of charge sample and resolution Δz.

The signal of the charge distribution is the integral of the deconvolution of the rectangular pulse field $e_p(t)$ and the rectangular space charge ρ(z) as shown in Equation(1) for the PEA method, while it is the deconvolution of the rectangular acoustic pulse p(t) and the rectangular space charge ρ(z) as shown in Equation(4) for the PWP method [3]. In other words, the signal waveforms are not the ideal rectangular shape, but trapezoidal. Moreover, as the charges on the electrodes are surface charges without width, the signal waveforms from the surface charges are rectangular in shape with a limited width. Finally, according to the rule of the total charge has to be zero in a closed circuit, the sum of the space charge in the sample and the surface charges on the electrodes must be zero. The total area of the three kinds of charges is also zero.

Next, let us compare the resolutions of the four kinds of signal waveforms. In case (a)Δz/d=1%, the signal surface charge is very large and the space charge signal in the sample is extremely small compared to the surface charge signal. In this case, if the surface-charge and the space-charge signals are displayed on the same screen, it is difficult to observe the space charge. In case (d) Δz/d=8%, the width of the surface-charge signal becomes wider and the space-charge signal in the sample becomes a trapezoid, which is quite different from the rectangular shape of the original space-charge distribution. For this reason, it is necessary to decide how much relative spatial resolution (% space resolution) measurement should be given. According to experience, setting the relative space resolution between 2% to 5% is a general selection. Generally, an indication of the spatial resolution of a charge distribution with 1 μm or 50 μm (absolute space resolution) is not enough; the thickness of the sample should also be indicated. In other words, it is better to use relative resolution to describe a measurement. Of course, the higher the absolute resolution, the better is the measurement. In fact, for thin sample, one always seeks the highest absolute resolution, but even in this case, the relative resolution to describe the experimental results can also be used..

(2) Sample Thickness and Pulse Duration for PEA Method

Assume the thickness of the sample is d and the duration of the pulse voltage is ΔT_p. The relative spatial resolution η is given in Equation (5). The term d/u_{sa} in the denominator is the transit time at which the acoustic pulse propagates through the sample. Here, u_{sa} is the acoustic velocity of the sample. For a polyethylene sample, a typical acoustic velocity is 1950 m/s.

$$\eta = \frac{\Delta T_P}{d/u_{sa}} \times 100\% \tag{5}$$

The acoustic velocities for other insulation materials are shown in Table 2.

The relationship between the thickness d of the sample and duration ΔT_p of the pulse voltage is shown in Figure 8 according to Equation (5). The use of this figure to decide the resolution is now explained. Figure 8 shows the linear relationship of the thickness d of the sample and the duration ΔT_p of the pulse voltage in Equation (1).

Table 2: Physical properties of piezoelectric transducers, dielectrics and metals

Material	Density ρ [kg/m^3]	Acoustic velocity u [m/s]	Acoustic impedance Z(= ρ u) [kg/m^{2}sec]	Relative dielectric constant ε_r	Piezoelectric constant	
					h(τ)(=d(τ)) [m/V]	g(τ) [C/m^2]*
Quartz (SiO_2)	2650	5740	15.2×10^6	4.5	2×10^{-12}	20.0
$LiNbO_3$	4700	7360	34.4×10^6	28	60×10^{-12}	4.0
$LiNbO_3$ - n	4700	7360	34.4×10^6	28	–	–
PZT-4	7500	4600	34.5×10^6	1300	289×10^{-12}	40.0
PVDF - α	1780	2260	4.0×10^6	13	–	–
PVDF - β	1780	2260	4.0×10^6	13	18×10^{-12}	6.4
PVDF-TrFE	1880	2400	4.5×10^6	13	17×10^{-12}	6.8
PMMA	2310	2680	6.2×10^6	2.6	–	–
PE	930	1950	1.8×10^6	2.3	–	–
Aluminum	2690	6420	17.3×10^6	–	–	–
Brass	8600	4700	40.6×10^6	–	–	–
Semiconducting material	990	1950	1.9×10^6	–	–	–

*$g(\tau)=\varepsilon_0\varepsilon_r / d(\tau)$

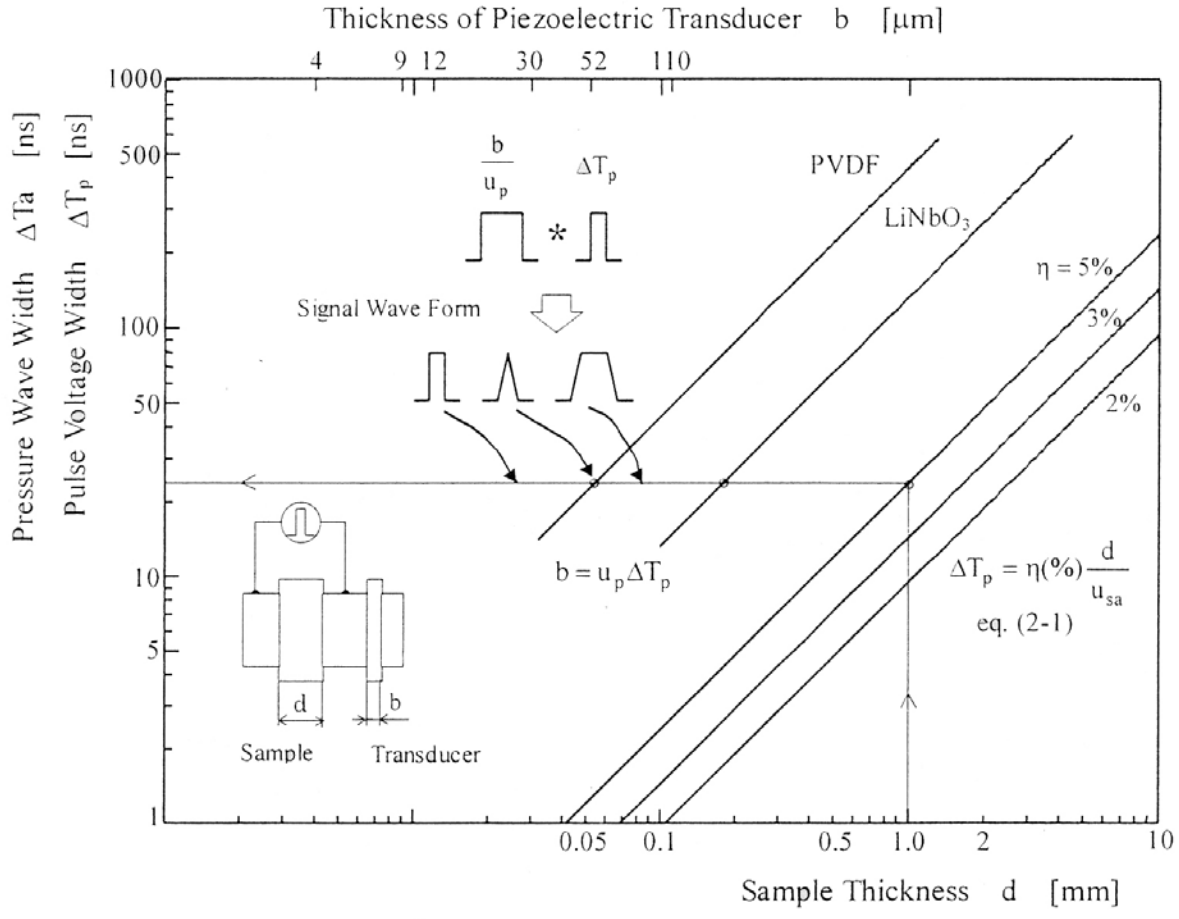

Figure 8: Relationship between sample thickness d and pulse voltage width ΔTp & relationship between pulse pressure width ΔTa and transducer thickness b.

In the PEA method, as the acoustic pulse is detected by a transducer, there is an additional deconvolution of the acoustic pulse p(t) from electric charge and transducer h(τ) for the charge signal detection q(t) as shown in Equation (2). The spatial resolution is also affected by the thickness b of the transducer . If the transducer is very thin, its influence on the resolution becomes less.

For example, for a relative resolution of 5% for a 1.0 mm thick polyethylene, PE, sample, the duration of the pulse voltage is 25 ns according the linear relation shown in Figure (8). Furthermore, by using Equation (6), the duration of the pulse voltage can be determined, ΔT_p=25 ns, where the acoustic velocity in PE is 1950 m/sec.

$$\Delta \boldsymbol{T_p} = \eta \times \frac{\boldsymbol{d}}{\boldsymbol{u_{sa}}} = 0.05 \times \frac{10^{-3}}{1950} = 25 \times 10^{-9} = 25\ \boldsymbol{ns} \tag{6}$$

(3) Sample Thickness and Pulse Duration for PWP Method

For the PWP method, the acoustic pulse is generated by a pulse laser or a piezoelectric transducer. For either method, the acoustic pulse with duration ΔT_a can be substituted into Equation (7) to calculate the relative spatial resolution. Thus, it is only necessary to change the vertical axis in Figure 8 from the duration, ΔT_p, of the pulse voltage to the duration, ΔT_a, of the acoustic pulse, and then decide how much relative resolution required.

$$\eta = \frac{\Delta T_a}{d/u_{sa}} \times 100\% \tag{7}$$

In case of a spatial resolution of 2% ~ 5%, Equation (7) gives the relationship between the duration ΔT_a of the pressure pulse and the transit time d/u_{sa} of the acoustic pulse through the sample. For a 2 % spatial resolution of the space charge in a 1.0 mm thick PE sample, the duration of the acoustic pulse should be ΔT_a =10 ns, where the acoustic velocity in PE is 1950 m/sec. This duration of the acoustic pulse is very narrow, and can be obtained by using either laser pulse irradiation of the LIPP method or the piezo-electric transducer of the PIPWP method.

$$\Delta \boldsymbol{T_a} = \eta \times \frac{\boldsymbol{d}}{\boldsymbol{u_{sa}}} = 0.02 \times \frac{10^{-3}}{1950} = 10 \times 10^{-9} = 10\ \boldsymbol{ns} \tag{8}$$

3.2 High Voltage Circuit

(1) Selection of Coupling Capacitance The need for a coupling capacitance is first explained. If the coupling capacitance C_c does not exist, then the dc voltage will not be applied to the test sample for the PEA method as shown in Figure 1. In other words, the HV electrode is grounded via the inner resistance R_p of the pulse generator. Therefore, the pulse voltage applied to the sample is decided by the value of the series resistance R_{dc} (=10kΩ) and the internal resistance R_p (about 50Ω) of the pulse generator. As the internal resistance of the pulse generator is much smaller than series resistance R_{dc}, most of the dc voltage is applied to the series resistance R_{dc}, and not the sample. After a coupling capacitance C_c (several nF) is inserted between the pulse generator and the sample, the total equivalent parallel dc resistance of the coupling capacitance (over 10^{12}Ω) and the dc resistance of sample (10^{12} ~ 10^{15}Ω) is much larger than series resistance R_{dc} (=10kΩ) of the dc source. In this

case, most of the dc voltage can be applied to the sample.

The value of the coupling capacitance C_c must be chosen such that most of the pulse voltage $v_p(t)$ appears across the sample, $v_{sa}(t)$, For this to occur C_c should be much greater than the sample capacitance, C_{sa}, according to Equation (9),

$$v_{sa}(t) = v_p(t) C_C / (C_C + C_{sa}) \cong v_p(t) \tag{9}$$

This condition is satisfied using Equation (10).

$$C_C \geq 100 \times C_{sa} \tag{10}$$

The capacitance, C_{sa}, of the test sample can be calculated for PE (ε_r =2.3), d=1.0 mm and electrode area (S) of 4.0 cm².

$$C_{sa} = \frac{\varepsilon_0 \varepsilon_r S}{d} = \frac{8.854\times10^{-12} \times 2.3 \times 4 \times 10^{-4}}{10^{-3}} = 8.1\,\text{pF} \quad \text{so that} \quad C_C = 100 \times 8.1\,\text{pF} \approx 1000\,\text{pF} \tag{11}$$

The coupling capacitance should be chosen as C_C=1000 pF.

(2) Selection of Series Resistance The pulse voltage cannot be applied to the sample if the series resistance R_{dc} is not in the circuit. This is explained according to the measurement circuit for the PEA method shown in Figure 1. If R_{dc} is not in the circuit, the capacitance C_{sa} of the sample (~ several pF) and the equivalent capacitance of the dc power source (about several mF) are in parallel, and the total capacitance is several mF. Most of the pulse voltage will be applied to the coupling condenser C_c (~ several nF). Thus, the pulse voltage cannot be applied to the sample. If a suitable resistance R_{dc} is inserted into the circuit between the sample and the dc voltage source, the pulse voltage will be shared by capacitance C_{sa} of the sample and coupling capacitance C_c. Therefore, the pulse voltage can be applied to the sample as the value of C_c is much larger than that of C_{sa}.

The value of the series resistance R_{dc} is determined as follows: the pulse current from the pulse voltage flows into two directions, through sample C_{sa} and through the dc power source via the series resistance R_{dc}. Only the current that flows into the sample contributes to the space charge measurement. The value of the resistance R_{dc} should be large enough to allow most of the pulse current to flow into the sample rather than the dc power source. This condition is shown in Equation (12),where f_p is the main frequency component of the pulse voltage defined in Equation (14).

$$\frac{1}{2\pi f_p c_{sa}} \ll R_{dc} \tag{12}$$

The other role for the series resistance is to protect the dc power source and the electrodes if there is a breakdown in the sample. When a breakdown occurs, the dc high voltage is applied across the series resistance directly. In order to avoid surface discharge along the resistance, a long resistance (4 - 8 cm in length) is necessary.

Equation (12) can be rewritten as Equation (13), when the resistance of R_{dc} is 500 times larger than the impedance of sample capacitance C_{sa}

$$R_{dc} = 500 \times \frac{1}{2\pi f_p C_{sa}} \tag{13}$$

$$f_p = \frac{1}{2\,\Delta T_p} \tag{14}$$

As the pulse duration is ΔT_p = 25 ns, the minimum value of the dc series resistance from above equations is given by R_{dc} =50 kΩ.

$$f_p = \frac{1}{2 \times 25 \times 10^{-9}} = 2 \times 10^7 \text{ Hz} \tag{15}$$

$$R_{dc} = 500 \times \frac{2\Delta T_p}{2\,\pi\, C_{sa}} = 500 \times \frac{1}{2\pi \times 2 \times 10^7 \times 81 \times 10^{-12}} = 50 \text{ k}\Omega \tag{16}$$

3.3 Acoustic Signal and Transducer for PEA Method

(1) Detection of Acoustic Signal

The acoustic pulse is measured using a piezoelectric transducer. Figure 9 shows the measurement circuit of the acoustic pulse and the relationship between acoustic signal pulse p(t) and the charge signal q(t) generated from a piezoelectric function h(τ). The transducer is inserted between the two electrodes and the acoustic pulse propagates through the test sample and the ground electrode to the transducer. When the acoustic wave propagates through the transducer h(τ=z/u_p), an electric charge signal q(t) in the transducer is generated. This process is described in Figure 9 (a) as shown in the deconvolution of Equation (2) and rewritten in Equation (17). As shown in the same figure, the deconvolution equation shows that the acoustic pulse p(t-τ)u_pdτ within a tiny duration induces the electric charge with the amount of h(τ)p(t-τ)u_pdτ in the transducer. The induced charge signal q(t) is equal to the integral of this charge divided by the thickness b.

$$q(t) = \frac{2Z_p}{Z_{Al} + Z_p} \frac{u_p}{b} \int_{-\infty}^{+\infty} h(\tau)\, p(t-\tau)\, d\tau \tag{17}$$

Various induced charge signal waveforms q(t) are shown in Figure 9 (b)-(e) when the acoustic pulse p(t) (duration =ΔT_p) is detected by the transducer h(τ) (duration =b/u_p). In cases (b) and (c), as $\Delta T_p \le b/u_p$ (for a thick transducer), the measured induced charge signals q(t) do not show the waveform of the acoustic pulse p(t). For (d) and (e), as $\Delta T_p \ge b/u_p$ (for a thin transducer), the signal q(t) is approximates the waveform of the acoustic pulse p(t).

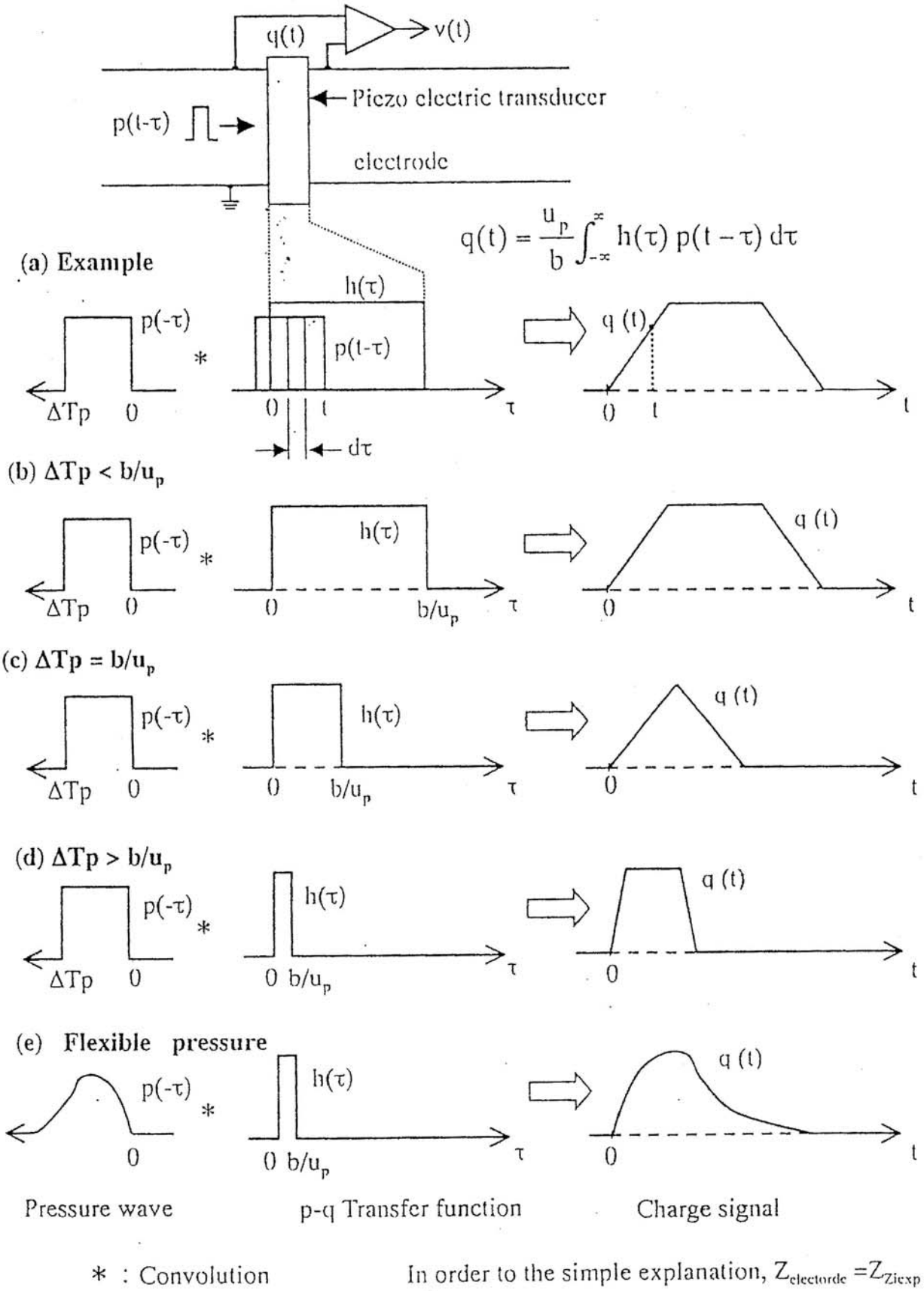

Figure 9: Measument principle of acoustic pulse generated by piezo-electric transducer. For simplification, the acoustic impedances of transducer, Zp, and both electrodes, ZAl, are assumed equal. "*" signifies deconvolution.

(2) Transducer Thickness

In the PEA method, the minimum duration of the acoustic pulse is equal to the duration of the applied electric pulse. The duration b/u_p of the transducer should be shorter than duration ΔT_p of the pulse voltage. In order to obtain a high relative spatial resolution (2 - 5%), firstly a narrow pulse should be selected, and secondly a thin transducer should be used.

Design Example: Thickness of Transducer for PEA

As mention above, the thickness b of the transducer can be determined using the condition of Equation (18), where ΔT_p is the duration of the pulse voltage and u_b is the sound velocity in the transducer.

$$\frac{b}{u_b} \le \Delta T_p \tag{18}$$

If a PVDF film is chosen as a transducer, in which the sound velocity is 2600 m/s, the thickness b of the transducer can be obtained. Then, the thickness of PVDF should be chosen as b=30 μm from

$$b \le \Delta T_p u_b = 25\times10^{-9}\times2600 = 65\,\mu m \tag{19}$$

(3) Acoustic Impedance Matching

In the case of a thin transducer, if the acoustic impedance between the transducer and the electrodes is different, there will be a reflection due to acoustic impedance mismatching. In this case, it is difficult to measure the electric charge signal q(t) without distorting the acoustic pressure wave. The reflection process is shown in Figure 10. First, when an acoustic pulse $p_0(t)$ propagates across the first interface (front interface) of the ground electrode and the transducer, part of it propagates through the interface and part of it is reflected. When the acoustic pulse comes out the transducer, the second reflection will occur at the second interface (rear interface) of the transducer and the aluminum electrode. The reflected acoustic pulse will cause many further reflections within the transducer and induces unnecessary charge on the surface of the transducer. The transmission ratio of the acoustic pulse at the interface is determined by the acoustic impedances of the materials used. An example of the ratio is shown in Figure 10.

If a backing absorber is inserted at the second interface (rear interface) between the transducer and the aluminum electrode, the multi-reflections can be avoided. For example, if an un-polarized material (αtype PVDF) with the same base material as the transducer (βtype PVDF) is attached at the rear of the transducer, the reflection can be avoided. Also the same situation can occur for a thin $LiNbO_3$ transducer. A backing material the same as the $LiNbO_3$ transducer should be used at the rear of the transducer to reduce the reflection. Only after the multi-reflections are omitted does the charge signal show the acoustic signal pulse. In practice, the reflection cannot be completely avoided. Therefore, a signal processing based on a convolution technique is used to remove the small multi-reflections as described in Session 4. The surface of the backing material should be coated by conducting paint to make an electrical connection between the transducer and the signal detecting electrode.

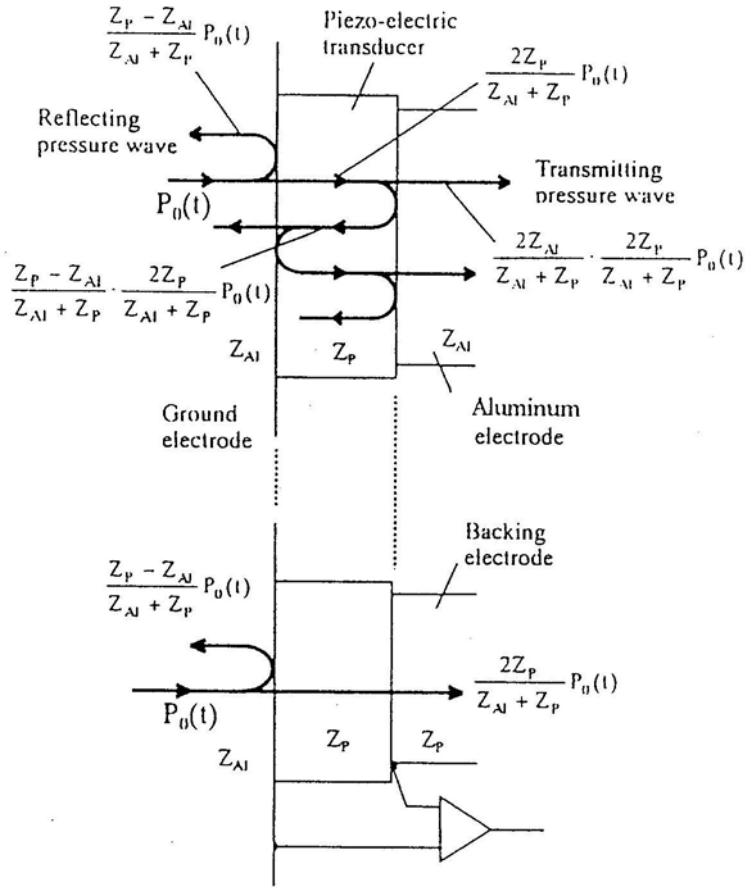

Figure 10: Multi-reflections of acoustic pulse at both surfaces of transducer and improving the multi reflection using a backing material.

Design Example: Acoustic Impedance Matching

The acoustic impedance Z_{tr} of the transducer should be equal to the acoustic impedance Z_{ba} of the backing material as shown in Equation (20). In the case of a PVDF-β transducer, the backing material should be PVDF-α (non-polarized), then Z(PVDF-β)=Z(PVDF-α). For a $LiNbO_3$ transducer, the backing material should be $LiNbO_3$-n (non-sensitive axis), then Z($LiNbO_3$)=Z($LiNbO_3$-n).

$$Z_{tr} = Z_{ba} \tag{20}$$

3.4 Acoustic Pulse Generation for PIPWP Method

The generation of a nanosecond acoustic pulse is difficult. The following methods are proposed:

(a) Application of an electric pulse to a transducer (PIPWP method)

(b) Irradiation of a pulse laser to a target electrode (LIPP method)

(1) Acoustic Pulse Generation using Transducer

Figure 11 shows the mechanism of the acoustic pulse generation when an electric field is applied to a transducer. After an electric field e(t) is applied to the transducer, the transducer is compressed and then a compression acoustic pulse $p_1(t)$ (transmitted towards the transducer) and an expansion pulse $p_2(t)$ (transmitted towards the electrode) are generated at the interfaces of the transducer and

the electrodes. Compression strain s(t) due to acoustic pulse $p_1(t)$ keeps increasing linearly until the acoustic pulse gets out the transducer. At this time, the strain reaches a maximum (saturation) and maintains this value until time t_1 at which the applied electric pulse decreases to zero. After t_1, the strain decreases linearly to zero. The strain s(t) and the acoustic pulse p(t) are shown in Equations (21) and (22). Here, a is the thickness of the transducer, $h(\tau)$ and $g(\tau)$ are the piezoelectric functions as shown in Table 2, u_g is the acoustic velocity, Z_g and Z_{Al} are the acoustic impedances of the transducer and the electrodes respectively.

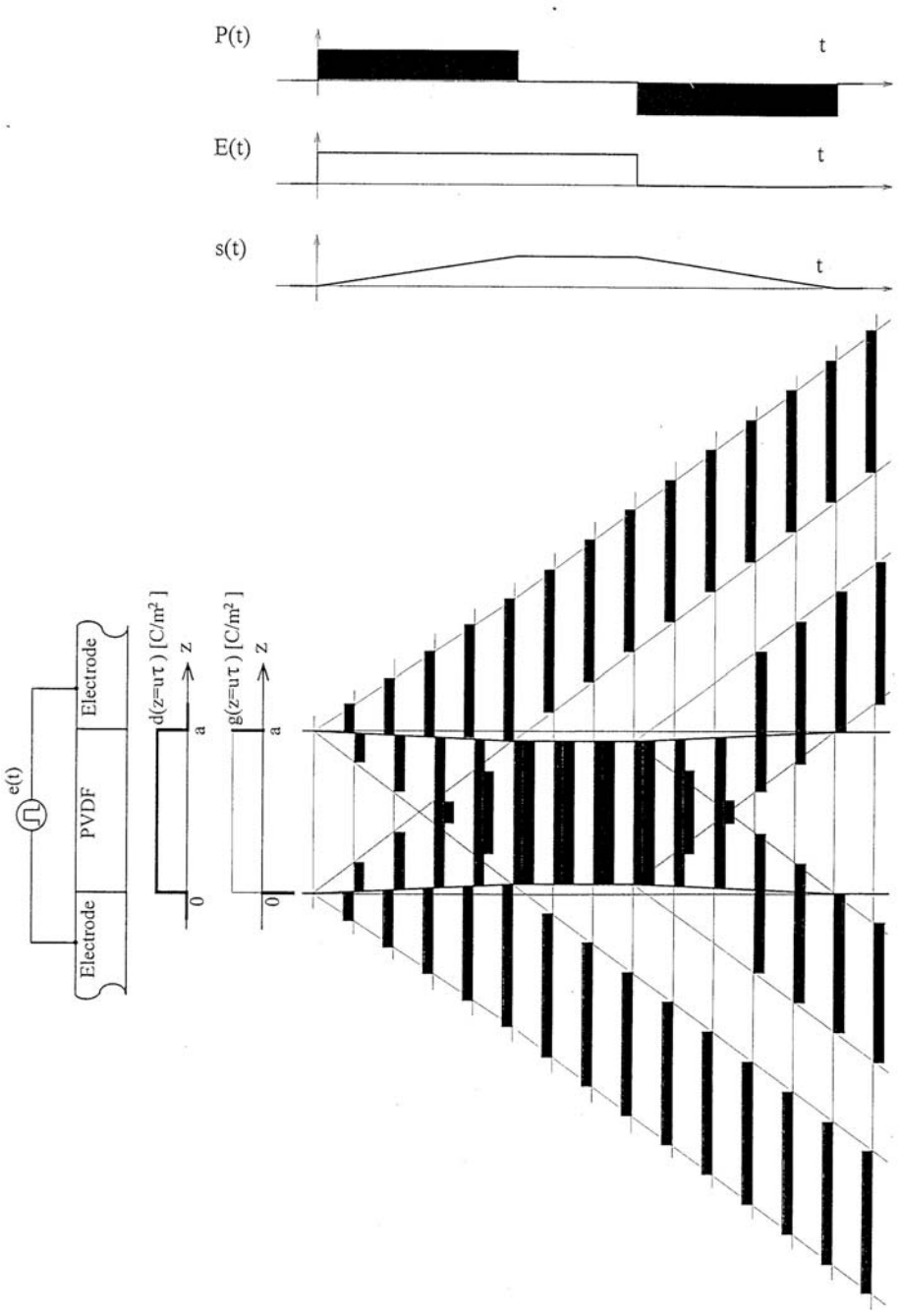

Figure 11: Explanation of generation of narrow pressure pulse by applicationof pulse voltage e(t) to piezo-electric transducer.

As shown in Equation (21), (22) and Figure 11, the acoustic pulse p(t) and the strain s(t) are time dependant. The maximum strain s_0 is the multiplication of the piezoelectric coefficient d [m/V] and the dc electric field E [V/m], i.e., $s_0 = d*E$. Until the strain reaches its maximum, the transducer is compressed continually (from 0 to a/u_g). As shown in Equation (21), the strain s(t) is the convolution of the piezoelectric function $d(\tau)$ and electric field $e(t-\tau)$. In the same figure, s(t) is described as the convolution of the piezoelectric function $d(\tau)$ with duration a and electric field e(t). These equations were also obtained under condition of acoustic matching between the transducer and the backing material of the signal detecting electrode.

$$s(t) = \frac{Z_{Al}}{Z_g + Z_{Al}} \frac{u_g}{a} \int_{-\infty}^{+\infty} d(\tau)\, e(t-\tau) d\tau \tag{21}$$

$$p(t) = \frac{Z_{Al}}{Z_g + Z_{Al}} \frac{u_g}{a} \int_{-\infty}^{+\infty} g(\tau)\, e(t-\tau) d\tau \tag{22}$$

The model of acoustic generation with a strain s(t) increase is explained as follow: Equation (22) shows an acoustic pulse p(t). The piezoelectric function $d(z=u_p\tau)$ [m/V] in Equation (21) is constant within the transducer as shown in Figure 11. However, the piezoelectric function $g(z=u_p\tau)$ [C/m^2] is positive and negative surface charges on the surfaces of the transducer at z=0 and z=a respectively. The acoustic pulse p(t) is generated by the two surface charges due to $g(\tau)$ when a pulsed electric field e(t) is applied to the transducer. This acoustic pulse acts on the two surface charges and the thickness of the transducer is changed. During the thickness changes, the expansion pulse and the compression pulse transmit towards the outside and inside the transducer respectively. The acoustic pulse stops generation after the compressed pressure is confined within transducer.

The component of the acoustic pulse generated at the interface of the transducer and the electrode travels towards the electrode and the transducer. The ratio transmitted to the electrode is shown in the first part of Equation (21) and (22) as an acoustic impedance ratio of the transducer and the electrode, where Z_{Al} is the acoustic impedance of the aluminum electrode and Z_g is that of the transducer. If the acoustic impedance at both sides is the same, then the ratio becomes 0.5. The waveform shown in Figure 11 is plotted by assuming that the acoustic impedance of the transducer is the same as that of the electrode.

(2) Acoustic Pulse Generation

The following three methods to generate a single acoustic pulse are explained as shown in Table 3.

(a) Short duration voltage applied to a thick transducer (square pulse pressure wave)

(b) Long duration voltage applied to a thin transducer (square pulse pressure wave)

(c) Short duration voltage applied to a thin transducer (oscillating pulse pressure wave)

The characteristics of the three methods are explained along with the generation method of the acoustic pulse and the selection standard of the transducer. Typical examples are given in Table 3.

Table 3: Selection of the thickness of the transducer and the duration of the electric pulse

Transducer	Thickness a [μ m]	Acoustic velocity u_p [m/s]	Transit time $\Delta T_t(=a/u_p)$ [ns]	Duration of pulse voltage ΔT_p [ns]	Conditions	Acoustic pulse	
						Duration ΔT [ns]	Intensity
(a) Thick $LiNbO_3$	8000	7360	1080	10	$\Delta T_t \gg \Delta T_p$	10	Weak
(b) Thin PVDF	26	2600	10	700	$\Delta T_t \ll \Delta T_p$	10	Strong
(c) Thin PVDF	26	2600	10	10	$\Delta T_t = \Delta T_p$	30	Strong

(a) Short Duration Voltage Applied to a Thick Transducer

The generation mechanism for this method is shown in Figure 12 (a). When a short duration electric field is applied to a thick transducer, two narrow acoustic pulses are generated at the surface of the transducer. One pulse is the expansion pulse and the other is the compression pulse. They travel through the transducer and keep the same relative time interval during the transmission. As only one of them is used when the space charge measurement is carried out, the time interval $\Delta T_t (=a/u_g)$ should be longer than the transit time $\Delta T_{sa} (=d/u_{sa})$ of the acoustic pulse that travels through the sample. However, as the thickness of the transducer increases, the electric field decreases (assuming that the applied pulse voltage is constant). For this reason, a strong acoustic pulse cannot be obtained.

(b) Long Duration Voltage Applied to a Thin Transducer

The generation mechanism for this method is shown in Figure 12 (b). When a long duration electric field is applied to a thin transducer, two narrow acoustic pulses are generated at the surfaces of the transducer. The positive acoustic pulse is generated when the pulse electric field turns on and the negative acoustic pulse is generated when the pulse electric field turns off. The duration of the acoustic pulse is $\Delta T_t (=a/u_g)$. If the duration ΔT_p of the pulse field is longer than the transit time ΔT_{sa} $(=d/u_{sa})$ of the acoustic pulse through the sample, one of the acoustic pulses can be used as the measurement pulse.

(c) Short Duration Voltage Applied to a Thin Transducer

The generation mechanism for this method is shown in Figure 12 (c). When a short duration electric field, ΔT_p, is applied to a thin transducer in which the transit time is $\Delta T_t(=a/u_g)$, oscillating narrow acoustic pulses are generated. The short duration of the voltage, ΔT_p, then equals the transit time $\Delta T_t(=a/u_g)$ through the transducer. From the generation mechanism of the pressure wave as mentioned above, the duration of the acoustic wave is three times the transit time $\Delta T_t(=a/u_g)$ and its wave shape is oscillatory. If the oscillating narrow acoustic pulses travel through the charged sample, the real charge profile is obtained after mathematical de-convolution processing as described in Session 4.

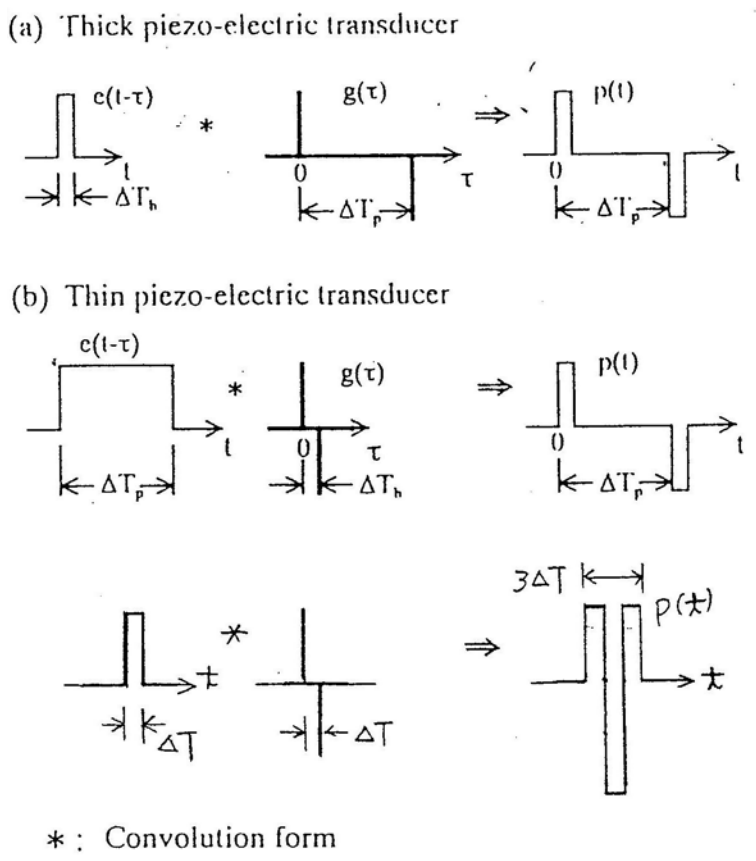

Figure 12: Mechanism to generating a narrow pressure pulse using piezo-electric transducer.

A feature of methods (b) and (c) is that a strong acoustic pulse is obtained as the transducer is thin and the electric field e(t) applied to the transducer is high, i.e., the generated acoustic pulse p(t) depends on the applied electric field e(t) as given in Equation (22) and also the piezoelectric function g(τ).

3.5 Acoustic Pulse Generation for LIPP method

Generally the acoustic pulse is generated by irradiating a pulse laser beam onto a target that is attached to one surface of the sample. A laser source often used in this method is a Nd:YAG laser. The targets used in this method are evaporated electrodes, metal plates and semi-conducting electrodes.

(1) Evaporated Electrodes

If a very thin evaporated electrode is used as a target, high resolution measurements can be carried out. However, as the evaporated electrode is easily damaged, a high power output laser cannot be used. Generally, an evaporated electrode is only used for a relative thin sample (10 μm to several 100 μm in thickness).

(2) Metallic Electrodes

This electrode is suitable for a high power output laser and thick samples (several 100 μm to several mm in thickness). The measurement can be repeated many times. Repeated measurement helps to reduce noise and enhance the signal to noise ratio (S/N).

(3) Semiconducting Electrodes

To analyze the effect of a semiconducting electrode or the effect of semiconductor material (polyethylene blended with pasted carbon) as used in a power cable, a semiconducting sheet can also be used as the target material. This target can be used repeatedly, but the spatial resolution is poor (over 50 μm) due to the attenuation and dispersion of the acoustic pressure pulse in the semiconducting material.

3.6 Nanosecond HV Pulse Generator

For the PEA method, a high voltage pulse is applied to the charged sample to generate the acoustic pressure pulse, whereas, for the PIPWP method, a high voltage pulse is applied to the transducer to generate the acoustic pulse. In both cases, a high voltage pulse generator in the nanosecond range is necessary. Table 4 shows the generation method, amplitude, duration, and repetition rate of the high voltage pulse. A discharging-type pulse generator using a coaxial cable is used for thick samples up to several mm thick, while a transistor switch-type pulse generator is employed for thin samples. Coaxial cable pulse generators are classified into two types, the Fletcher type and the Wagner type. The generation methods are described below.

Table 4: High voltage generator characteristics

<table>
<tr><td colspan="2" rowspan="2">High voltage pulse generation method</td><td colspan="3">Characters</td></tr>
<tr><td>Voltage pulse Output*</td><td>voltage pulse Duration**</td><td>Repetition frequency</td></tr>
<tr><td rowspan="4">Discharge type by using coaxial cable</td><td rowspan="2">Fletcher type (inner conductor charging)</td><td>$\frac{V_0}{2}$</td><td>$\Delta T_p = \frac{2L}{c/\sqrt{\varepsilon_r}}$</td><td rowspan="2">150 Hz</td></tr>
<tr><td>50 – 4,000 V</td><td>3 – 1,000 nsec</td></tr>
<tr><td rowspan="2">Wagner type (outer conductor charging)</td><td>V_0</td><td>$\Delta T_p = \frac{L}{c/\sqrt{\varepsilon_r}}$</td><td rowspan="2">150 Hz</td></tr>
<tr><td>100 – 8,000 V</td><td>3 – 500 nsec</td></tr>
<tr><td colspan="2">Transistor switch</td><td>50 – 2,000 V</td><td>5 – 1,000 ns</td><td>2 – 3kHz</td></tr>
</table>

*: the maximum output of the pulse generator is limited by the withstand voltage of the relay switch.

**: the minimum duration of the pulse is limited by the pulse generation technique; the maximum duration is limited by the distortion of the waveform from the losses in he cable.

(1) Fletcher Type Pulse Generator

Figure 13 shows the principle of a Fletcher-type generator. The inner conductor of the coaxial cable on the right-hand side is connected to a HV power source V_0 via a large resistor R_0 (= 100kΩ). When the switch, SW, on the left-hand side is turned on, the charged cable starts to discharge through the load resistor R, and a voltage pulse is generated. The voltage waveform $V_1(t)$ at the load resistor R and voltage $V_2(t)$ at the voltage source end of the cable are also shown in Figure 13. When SW is on,

the voltage at the load resistor R(=Z_0, the characteristic impedance of the coaxial cable) becomes $V_0/2$ due to the voltage division between R and Z_0. The voltage pulse travels along the cable and reaches the right side, where, as Z_0<<R, the voltage pulse will be completely reflected towards the load resistor R againΩ. As the impedance on the left-hand side is matched, the voltage pulse is not reflected at this side. The discharge process is completed when the voltage pulse reaches this side and the pulse voltage returns to zero. From this figure, we know that the magnitude of the voltage pulse is $V_0/2$ and the duration is $\Delta T_p(=2\tau = 2L\sqrt{\varepsilon_r}/c)$, where τ is the transit time of an electromagnetic wave in the cable, L the length of cable, ε_r the relative dielectric constant, and c the velocity of light in space (= 3×10^8 m/sec).

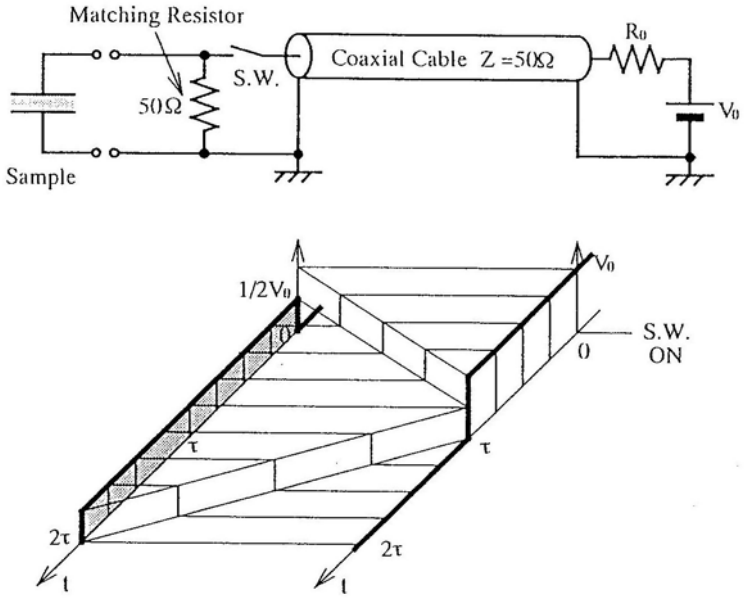

Figure 13: Circuit and HV pulse waveform of Fletcher type generator.

(2) Wagner Type Pulse Generator

Figure 14 shows the construction of the circuit of a Wagner-type generator and the waveform of the voltage pulse. The inner conductor of the coaxial cable is grounded via a load resistor R (=Z_0,, (the characteristic impedance of the coaxial cable). The outer conductors at the both ends of the cable are connected together and a negative HVDC voltage, -V_0, is applied to the outer conductors via a high resistance R_0, thus charging the coaxial cable. When switch SW is closed, a voltage pulse is generated at the load resistor. The waveform of the voltage pulse at the both end terminals is shown in Figure 14. $V_1(t)$ shows the waveform on the left-hand side and $V_2(t)$ shows the right-hand side waveform.

When SW is turned on, the potential of the outer conductor falls to zero. Potential $V_1(t)$ changes from zero to +V_0. Potential $V_2(t)$ changes from zero to +$V_0/2$ as the load resistor and the characteristic impedance of the cable are the same (R =Z_0). When the voltage pulse travels from the right to the left side within the cable, the pulse voltage at the left side is completely reflected as the left terminal is

open. After the reflection, the voltage pulse travels back through the cable and ends at the right side, when the discharge process is completed. As the left side is an open terminal, the reflection of the voltage pulse at this point makes the voltage change from V_0 to zero. As shown in Figure 14, a voltage pulse with duration $\Delta T_p (=\tau = L\sqrt{\varepsilon_r}/c)$ and magnitude V_0 is obtained.

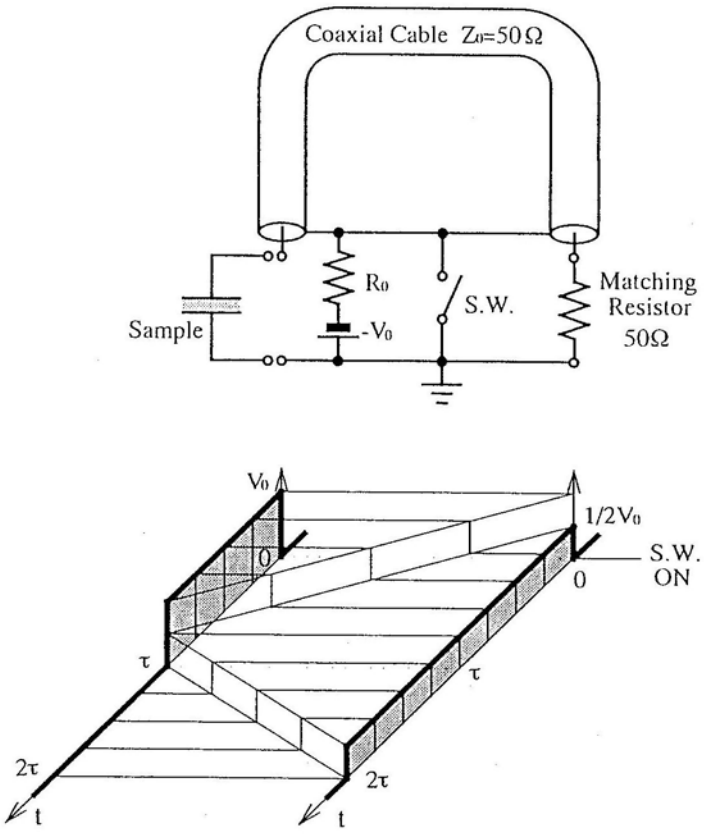

Figure 14: Circuit and HV pulse waveform of Wagner type generator.

(3) Pulse Generator, Comparison between Fletcher Type and Wagner Type

For a Fletcher-type generator, the voltage on the load resistor R is only half of the charging voltage V_0. This is due to the characteristic impedance Z_0 (=50Ω) of the coaxial cable being the same as the load resistor R (=50Ω). For Wagner-type generator, the output pulse voltage at the open terminal is the same as the charging voltage V_0, as shown in Table 4. Thus, a Wagner-type is selected if a high amplitude pulse voltage is needed, while a Fletcher-type is used if a wide duration pulse voltage is needed.

The pulse duration for the two methods is shown in Table 4 when the length of the charged coaxial cable is L [m]. Here, c ($=3.0\times10^8$ m/sec) is the velocity of light in space, and ε_r (=2.3) is the relative dielectric constant of the coaxial cable. For a Fletcher-type switch, as the voltage pulse is reflected at the right terminal, the duration is twice that of a Wagner type.

(4) High Voltage Relay Switch

The switch (SW) used in Figure 13 and Figure 14 should be a HV switch without chatter. Nowadays, use is made of a mercury relay and reed relay filled with an electronegative gas. A reed relay is a mechanical relay working at a repetition rate of about 150 Hz. Its lifespan is about 10^5 operations.

(5) Fast High Voltage Transistor Switches (FHTS)

As the voltage signal of a space charge distribution is very weak, only several tens of microvolts, a signal averaging technique is generally employed to increase S/N when a digitizing oscilloscope is used to measure the signal. For this purpose, a HV pulse generator that can generate a repetitive pulse with a given frequency is necessary. For the discharge-type generator mentioned above, the maximum repeat frequency is about 150 Hz, while for the FHTS type generator, the maximum frequency is about 3 kHz. For a short duration space charge measurement in the order milliseconds, a FHTS is a better choice.

Figure 15 shows the basic circuit and the signal waveform using the FHTS. The principle is that after capacitor C is charged, the FHTS switch lets the charge on the capacitor discharge via R_3 and R_4 within a given time interval (the duration of the HV pulse). The relationship between the trigger voltage (5V) and the output pulse voltage (2000V level) is also shown in Figure 15. The duration of the output pulse is determined by the particular FHTS. The level of the output HV pulse is variable according to the amplitude of the high voltage power source used. The frequency is determined by the frequency of the trigger signal.

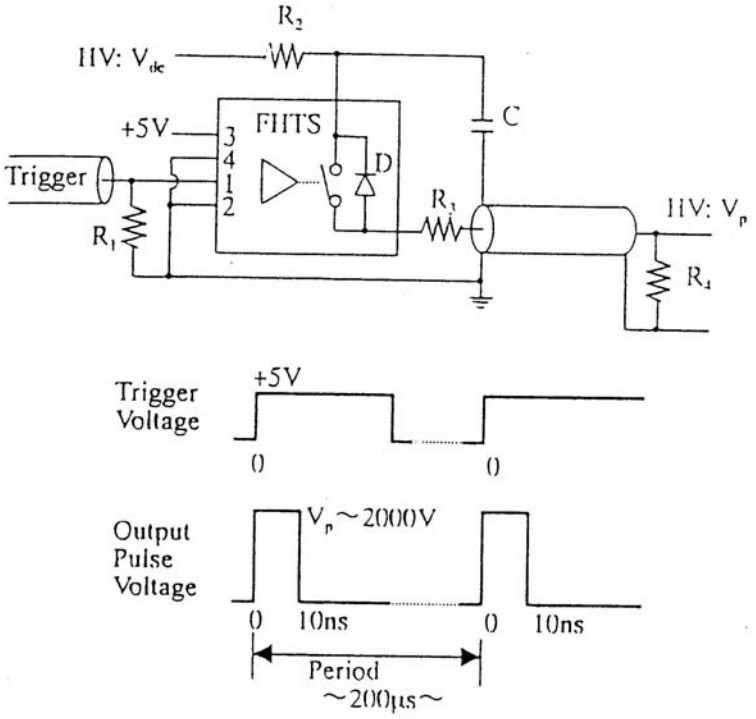

Figure 15: Circuit and waveform of nanosecond pulse generator using a FHTS.

3.7 Shielding from Electric Noise

As the signal level of the charge signal is typically 10-100 μV, a high gain amplifier (about 40 dB) is necessary. When a nanosecond voltage pulse is applied to the sample during the measurement, there is a lot of high frequency electromagnetic noise radiated into the space around the sample. For this reason, the transducer and the amplifier should be shielded perfectly in a metal case. Furthermore, the noise also interferes with the coaxial cable carrying the signal to the oscilloscope and also the leads connecting the dc source used to power the signal amplifier, so that perfect shielding for these lines are also necessary.

4. De-convolution Processing and Charge Calibration for Pulse Acoustic Method

The method to recovery a deformed signal waveform and how to calibrate in terms of electric charge are outlined in this section.

4.1 PEA method [3]

(1) De-convolution Processing

First, apply a low voltage V_{dc} to the sample and make sure no space charge is accumulated in the sample, and then measure the voltage signal v(t) from the surface charge σ(0) and σ(d). Pay attention to the first voltage signal $v_0(t)$ as shown in Figure 16 (c) that comes from surface charge $\sigma_0(0)$ only. By Fourier Transform, the voltage signal $V_0(f)$ is obtained as shown in Equation (25) and Figure 16 (d). $\sigma_0(0)$ is a surface charge and can be calculated according to Equation (26) by the application of a dc voltage V_{dc}. Thus, S(f) can be calculated by substituting $V_0(f)$ and $\sigma_0(0)$ into Equation (25).

Second, apply a test voltage to the sample to generate some space charge in the sample, and then measure the voltage signals v(t), as shown in Figure 16 (a), from surface charge σ (0) and σ (d) and space charge ρ(z). By Fourier Transform, the voltage signal V(f) is obtained as shown in Equation (23) and Figure 16 (b). Equation (27) is obtained by substituting S(f) into Equation (23). As Equation (27) shows the charge distribution in the frequency domain, the waveform of the charge distribution σ (0), ρ(=$u_{sa}\tau$) and σ (d) as shown in Figure 16 (f) can be obtained by performing an inverse Fourier Transform.

$$V(f) = S(f)\left[\frac{\sigma(0)}{u_{sa}\Delta\tau} + R(f) + \frac{\sigma(d)}{u_{sa}\Delta\tau}\exp\left(-j2\pi f\frac{d}{u_{sa}}\right)\right] \tag{23}$$

$$S(f) = \frac{A(f)W(f)H(f)}{C_p}\frac{2Z_p}{Z_{Al}+Z_p}\frac{Z_{Al}}{Z_{sa}+Z_{Al}}\frac{u_{sa}u_p\Delta\tau^2}{b}E(f) \tag{24}$$

$$V_0(f) = S(f)\frac{\sigma_0(0)}{u_{sa}\Delta\tau} \tag{25}$$

$$\sigma_0(0) = \varepsilon_0\varepsilon_r\frac{V_{dc}}{d} \tag{26}$$

$$\left[\frac{\sigma(0)}{u_{sa}\Delta\tau}+R(f)+\frac{\sigma(d)}{u_{sa}\Delta\tau}\exp\left(-j2\pi f\frac{d}{u_{sa}}\right)\right]=\varepsilon_0\varepsilon_r\frac{V_{dc}}{d}\times\frac{1}{u_{sa}\Delta\tau}\times\frac{V(f)}{V_0(f)}\times F(f) \tag{27}$$

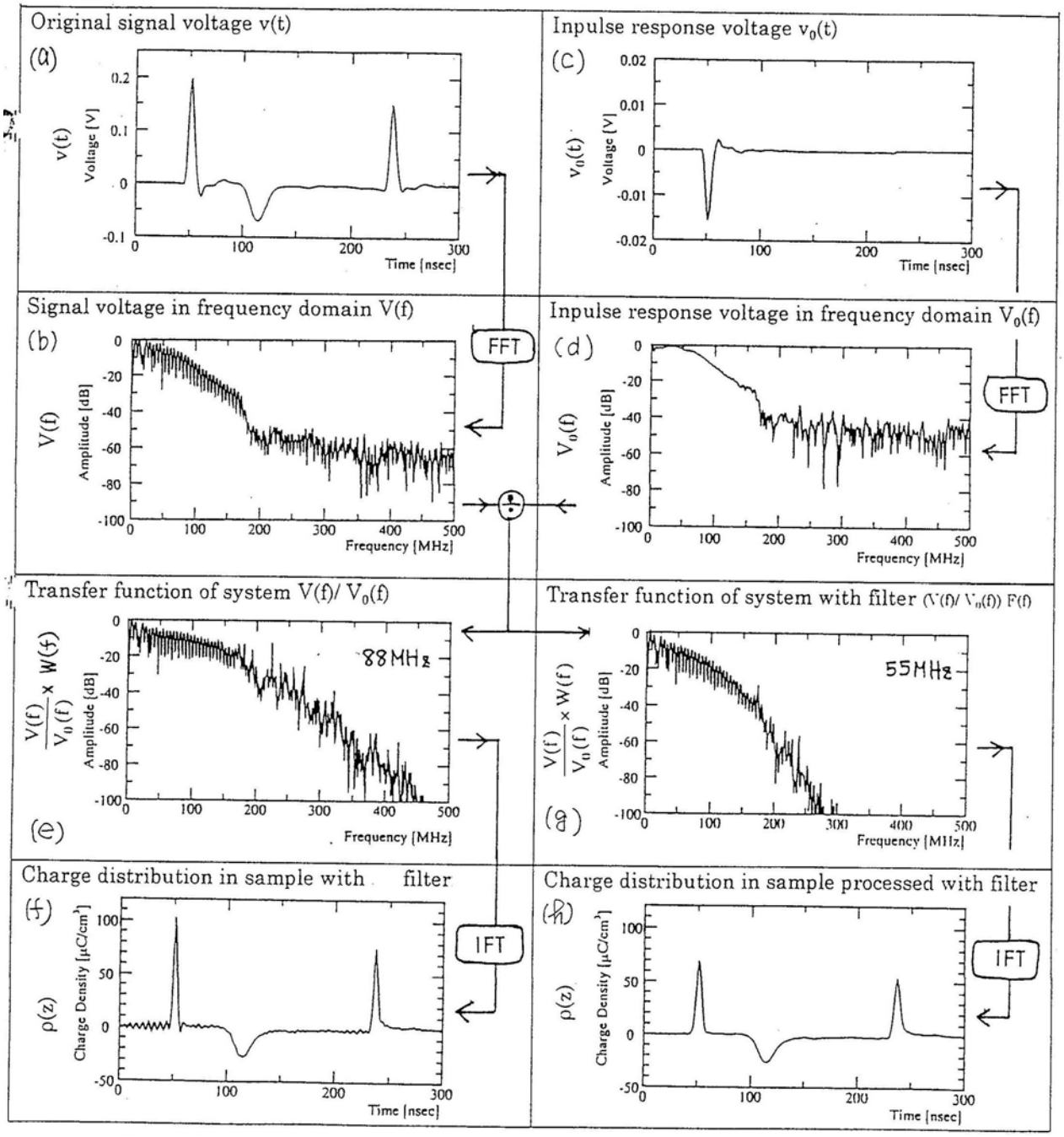

Figure 16: Recovery process of deformed signal waveform and charge calibration for PEA method.

(2) Charge Calibration

The left-hand side of Equation (27) shows the charge distribution in the sample in the frequency domain. On the right-hand side the term $V(f)/ V_0(f)$ shows the normalized charge profile which can be calculated, the term $(\varepsilon_0\varepsilon_r V_{dc}/d)(1/u_{sa}\Delta\tau)$ shows the amount of charge per sampling interval position on the oscilloscope screen which can calculated from the known values. Attention must be paid to Equation (27) as the surface charge density is in the unit [C/m^2], while the space charge density is in the unit [C/m^3]. It is necessary to unify the unit for the two kinds of charges as they are displayed on the same screen. As shown in Equation (27), $\sigma(0)$ and $\sigma(d)$ are divided by the sampling interval $u_{sa}\Delta\tau$ and have the same units as the space charge.

Typical results of a de-convoluted electric charge profile are shown in Figure 16 (f) and (h). There have been processed with the Wiener filter function F(f) in which the cut-off frequency is 88 MHz and 55 MHz respectively. The Wiener filter function F(f) is usually used to reduce the noise on the charge signal profile caused by the deconvolution process.

An example in Annex A illustrates the difficulties that can occur in multilayer test specimens that have different acoustic impedances. Reflected signals from interfaces can introduce unwanted signals on the space charge profile that may be incorrectly interpreted as space charges in the insulation.

4.2 PWP Method

The method to calculate the system function S(f) as shown in Equation (29) and the method to calibrate the charge are outlined in this section.

(1) De-convolution Processing

First, apply a low voltage V_{dc} to the sample and make sure no space charge is accumulated in the sample, and then measure the current signal i(t) from the surface charge $\sigma(0)$ and σ (d). Attention must be paid to the first current signal $i_0(t)$ that comes from surface charge $\sigma_0(0)$ only. By Fourier Transform, the current signal $I_0(f)$ is obtained as shown in Equation (30) and Figure 17 (d). $\sigma_0(0)$ is the surface charge and can be calculated from Equation (31) by applying dc voltage V_{dc} to the sample. Thus, S(f) can be calculated by substituting $I_0(f)$ and $\sigma_0(0)$ into Equation (30).

Second, apply a test voltage to the sample to generate some space charge in the sample, and then measure the current signals i(t), as shown in Figure 17 (a), from the surface charge σ (0) and σ (d) and space charge $\rho(z)$. By Fourier Transform, the voltage signal I(f) is obtained as shown in Equation (28) and Figure 17 (b). Equation (32) is obtained by substituting system function S(f) into Equation (28). As Equation (32) shows the charge distribution in the frequency domain, the profile of the charge distribution σ (0), $\rho(=u_{sa}\tau)$ and σ (d) as shown in Figure 17 (f) can be obtained by performing an inverse Fourier Transform.

$$\boldsymbol{I}(\boldsymbol{f}) = \boldsymbol{S}(\boldsymbol{f})\left[\frac{\sigma(0)}{\boldsymbol{u_{sa}}\Delta\tau} + \boldsymbol{R}(\boldsymbol{f}) + \frac{\sigma(\boldsymbol{d})}{\boldsymbol{u_{sa}}\Delta\tau}\exp\left(-\boldsymbol{j}2\pi\ \boldsymbol{f}\frac{\boldsymbol{d}}{\boldsymbol{u_{sa}}}\right)\right] \tag{28}$$

$$S(f) = \frac{A(f)W(f)G(f)}{Y} \frac{2Z_{sa}}{Z_{Al} + Z_{sa}} \frac{Z_{Al}}{Z_p + Z_{Al}} \frac{u_p \Delta\tau}{a} \frac{u_{sa}}{d} u_{sa} \Delta\tau \, E(f) \tag{29}$$

$$\boldsymbol{I_0(f) = S(f) \frac{\sigma_0(0)}{u_{sa} \Delta\tau}} \tag{30}$$

$$\sigma_0(0) = \varepsilon_0 \varepsilon_r \frac{\boldsymbol{V_{dc}}}{\boldsymbol{d}} \tag{31}$$

$$\left[\frac{\sigma(0)}{\boldsymbol{u_{sa}} \Delta\tau} + \boldsymbol{R(f)} + \frac{\sigma(\boldsymbol{d})}{\boldsymbol{u_{sa}} \Delta\tau} \exp\left(- \boldsymbol{j} 2\pi \boldsymbol{f} \frac{\boldsymbol{d}}{\boldsymbol{u_{sa}}} \right) \right] = \varepsilon_0 \varepsilon_r \frac{\boldsymbol{V_{dc}}}{\boldsymbol{d}} \times \frac{1}{\boldsymbol{u_{sa}} \Delta\tau} \times \frac{\boldsymbol{I(f)}}{\boldsymbol{I_0(f)}} \times \boldsymbol{F(f)} \tag{32}$$

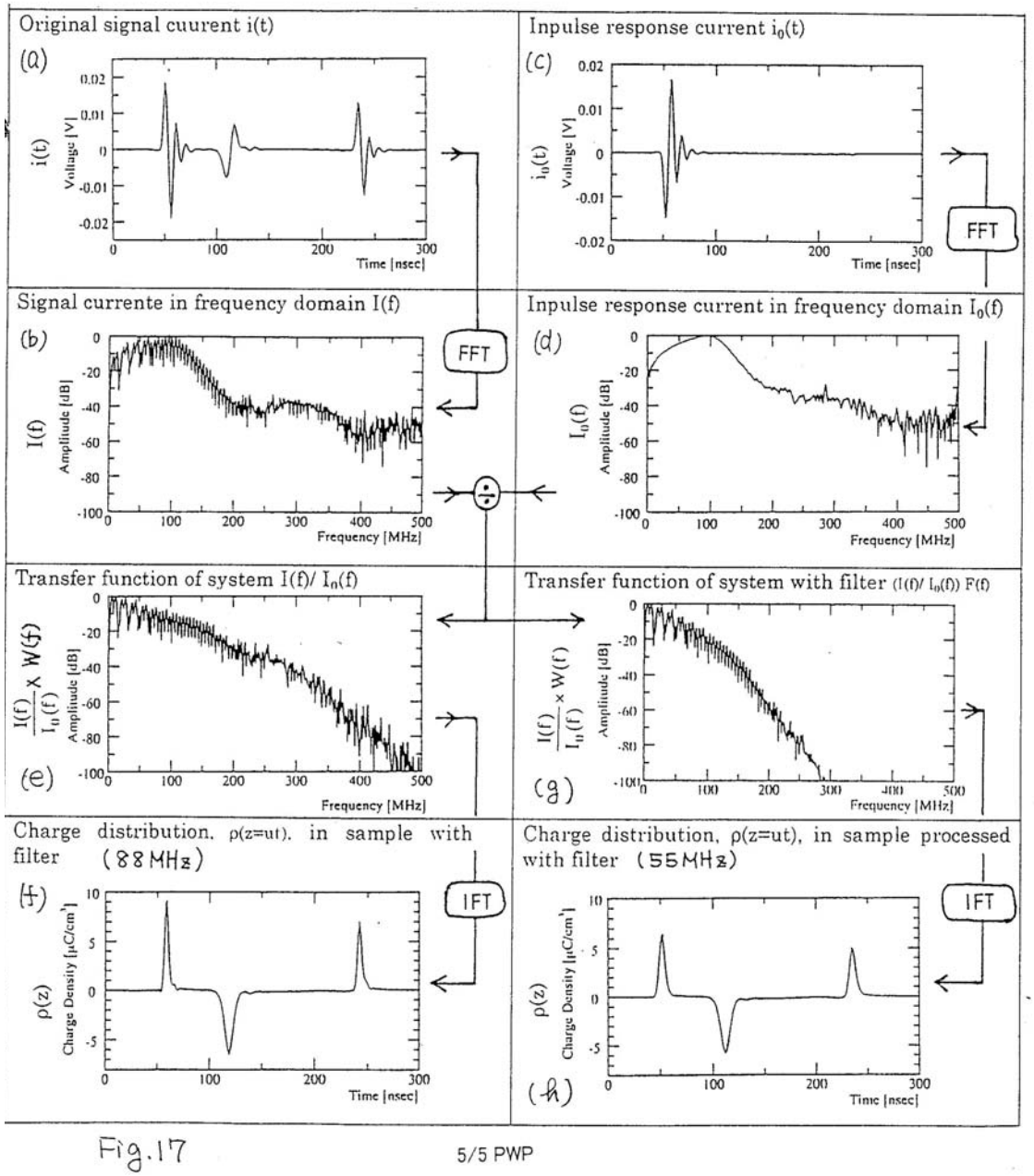

Fig.17

5/5 PWP

Figure 17: Recovery process of deformed signal waveform and charge calibration for PWP method.

(2) Charge Calibration

The left-hand side of Equation (32) shows the induced surface charge σ(0) , σ (d) and space chargeρ(z) in the sample in the frequency domain. On the right-hand side the term I(f)/I_0(f) shows the normalized charge profile which can be calculated, term ($\varepsilon_0\varepsilon_r V_{dc}$/d)(1/$u_{sa}\Delta\tau$) shows the amount of charge per sampling interval position on the oscilloscope screen which can calculated from the known values. Attention must be paid to Equation (32) as the surface charge density is in the unit [C/m^2], while the space charge density is in the unit [C/m^3]. It is necessary to unify the units for the two kinds of charges as they are displayed on the same screen. As shown in Equation (32), σ(0) andσ(d) are divided by the sampling interval $u_{sa}\Delta\tau$ and have the same units as the space charge.

Typical results of a deconvoluted charge profile are shown in Figure 17 (f) and (h). They have been processed with the Wiener filter function F(f) in which the cutoff frequency is 88 MHz and 55 MHz respectively. The Wiener filter function F(f) is usually used to reduce the noise on the charge signal profile caused by the deconvolution process.

5. Space Charge Measurement by the Thermal Step Method

5.1 Principle of Thermal Step Method

(1) Short Circuit Conditions

Consider an insulating sample of thickness d and surface area S provided with two conducting electrodes of abscissa x = 0 and, respectively, x = d (*Fig.18.a*). The material is considered homogeneous and infinitely plane ($\boldsymbol{d} \ll \sqrt{\boldsymbol{S}}$); thus, the electric field is assumed constant in any plane parallel to the electrodes. The sample is placed in a short circuit at a temperature T_0.

Because the system consisting of sample, electrode and conducting wire is in electrostatic equilibrium, a charge Q_i situated in the bulk of the insulator at an abscissa x_i induces charges of Q_1 and Q_2 at the electrodes. The dependence of the induced charges on the space charge Q_i and on the geometrical dimensions of the sample can be obtained with the aid of the short circuit conditions $\int_0^d \boldsymbol{E}(\boldsymbol{x})\boldsymbol{dx} = 0$, the electric charge conservation law $\boldsymbol{Q}_1 + \boldsymbol{Q}_2 + \boldsymbol{Q}_i = 0$ and the conservation of the electric displacement at the electrode/dielectric interfaces $\boldsymbol{div_S}\left(\varepsilon\vec{\boldsymbol{E}}\right) = \boldsymbol{Q}/\boldsymbol{S}$:

$$\boldsymbol{Q}_1 = -\frac{\boldsymbol{d}-\boldsymbol{x}_i}{\boldsymbol{d}}\boldsymbol{Q}_i\,,\ \boldsymbol{Q}_2 = -\frac{\boldsymbol{x}_i}{\boldsymbol{d}}\boldsymbol{Q}_i \tag{33}$$

If a temperature step $\Delta\boldsymbol{T} = \boldsymbol{T} - \boldsymbol{T}_0$ is applied to one face of the specimen (*Fig. 18.b*), the propagation $\Delta\boldsymbol{T}(\boldsymbol{x},\boldsymbol{t}) = \boldsymbol{T}(\boldsymbol{x},\boldsymbol{t}) - \boldsymbol{T}_0$ of the thermal front across the sample will give rise to local variations of the permittivity and the thickness (expansion or contraction), which can be written (in the first order):

$$\varepsilon = \varepsilon_{\boldsymbol{T}_0}\left(1+\alpha_\varepsilon\Delta\boldsymbol{T}\right),\ \boldsymbol{dx} = \boldsymbol{dx}_0\left(1+\alpha_{\boldsymbol{d}}\Delta\boldsymbol{T}\right) \tag{34}$$

where α_ε is the rate of change of the material permittivity with the temperature and α_d its rate of thermal expansion,

$$\alpha_\varepsilon = \frac{1}{\varepsilon}\frac{d\varepsilon}{dT},\quad \alpha_d = \frac{1}{x}\frac{dx}{dT} \tag{35}$$

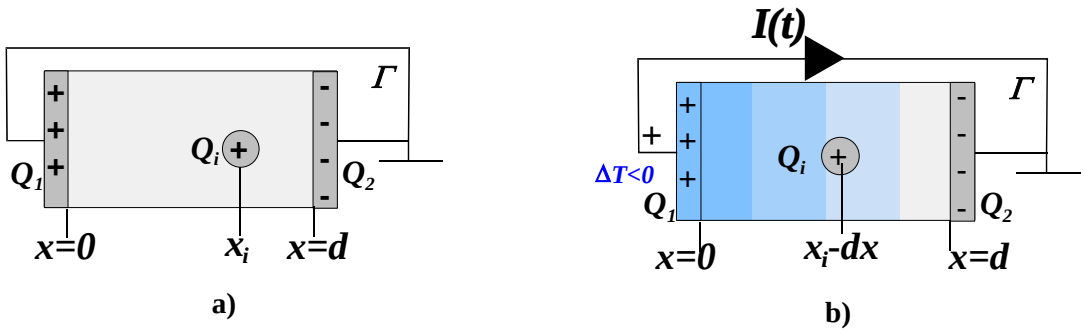

Figure 18: Principle of the TSM under short-circuit conditions:
(a) sample at equilibrium at T_0, (b) application of a thermal step.

The variations of the thickness and permittivity modify the induced charges, which can be written:

$$Q_1(t) = -Q_i \int_{x_i}^{d} \frac{dx}{\varepsilon(x,t)} \Big/ \int_0^d \frac{dx}{\varepsilon(x,t)},\quad Q_2(t) = -Q_i \int_0^{x_i} \frac{dx}{\varepsilon(x,t)} \Big/ \int_0^d \frac{dx}{\varepsilon(x,t)} \tag{36}$$

Using the previous notations and by putting:

$$\alpha = -\frac{1}{C}\frac{dC}{dT} \approx \frac{1}{x}\frac{dx}{dT} - \frac{1}{\varepsilon}\frac{d\varepsilon}{dT} = \alpha_d - \alpha_\varepsilon, \tag{37}$$

we get for $Q_2(t)$ the expression:

$$Q_2(t) = -Q_i \frac{x_i}{d}\left[1 + \frac{\alpha}{x_i}\int_0^{x_i} \Delta T(x,t)dx - \frac{\alpha}{d}\int_0^d \Delta T(x,t)dx\right] \tag{38}$$

The variation of the induced charges is reflected in the external circuit by the appearance of a current $I(t)$, called the thermal step (TS) current:

$$I(t) = -\frac{dQ_2(t)}{dt} \tag{39}$$

If the value of the TS current and the spatial distribution of the temperature are known for every instant t, the value of the charge Q_i and its position x_i can be determined.

In general, by defining $\rho(x) = \partial D(x)/\partial x = \varepsilon \partial E(x)/\partial x$ as the volume charge density at the abscissa x in a flat layer of thickness dx, it can be shown by integration over the entire sample [26] that the total current in the external circuit:

$$I(t) = -\alpha C \int_0^d E(x)\frac{\partial \Delta T(x,t)}{\partial t}dx \tag{40}$$

where $E(x)$ is the electric field at thickness x and C is the capacitance of the sample before the application of the TS. As shown by equation (40), the TS current amplitude is a function of the amount of charge stored in the sample, its distribution, the material parameters, and the

temperature derivative $\partial\Delta T(x,t)/\partial t$. In practice, the value of the TS current has a value between 1 pA and 1μA.

The temperature derivative is given by the heat equation for a plane geometry $\frac{\partial^2 \Delta T(x,t)}{\partial x^2} = W \frac{\partial \Delta T(x,t)}{\partial t}$, where $W = \mu c/\lambda$ is the reciprocal of the thermal diffusivity of the material, with μ the volume density of the insulation, c its specific heat and λ its thermal conductivity. The thermal loss between the sample and the radiator which produces the temperature variation can be taken into account by a so-called "equivalent-added thickness" x_0: the thickness x_1 of the different interfaces, of mean reciprocal thermal diffusivity W_1, is considered as equivalent to a layer x_0 having a reciprocal thermal diffusivity W_0 of the insulation: $W_1 x_1^2 = W_0 x_0^2$. The limits of the thermal step current integral (0 and d) can therefore be replaced by x_0 and x_0+d (the electric field across x_0 is assumed as zero):

$$I(t) = -\alpha C \int_{x_0}^{x_0+d} E(x) \frac{\partial \Delta T(x,t)}{\partial t} dx \qquad (41)$$

(2) Under Applied DC Voltage

For measurements under DC field, the setup described in Fig. 19 presents two major disadvantages:

- the current amplifier must not be in contact with the high voltage source;
- if a setup with the current amplifier placed between the sample and the ground is used (as for e.g., conduction current measurements), the conduction and the polarization currents are likely to mask the TS current.

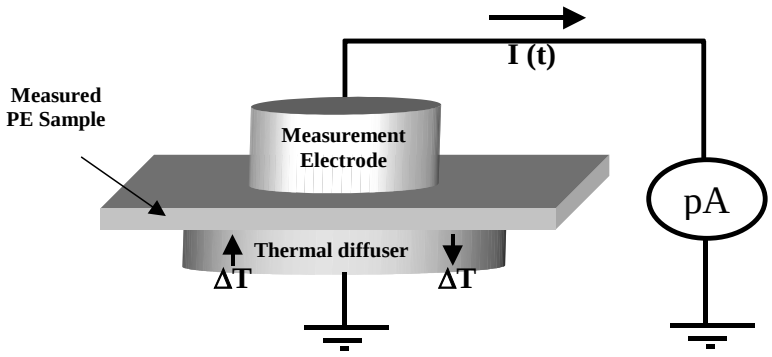

Figure 19: Experimental setup for TSM under short circuit conditions.

A solution to these problems is a "compensation sample", of identical dimensions as the test specimen and placed opposite to the latter (Fig. 20).

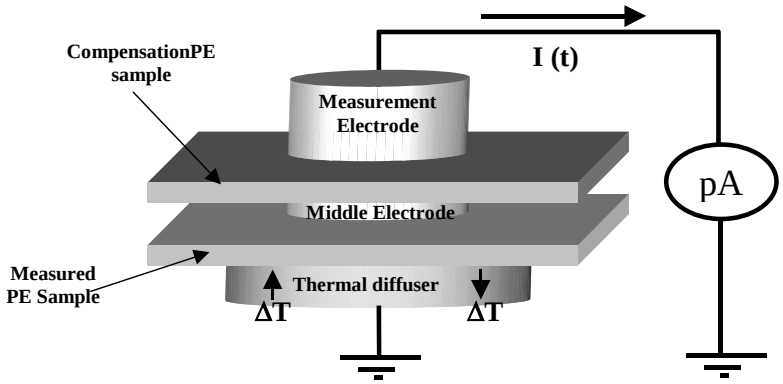

Figure 20: Principle of the "double capacitor".

By connecting one side of the compensation sample to the current amplifier and the other to the test specimen via an electrode, a "double capacitor" is obtained. A voltage then can be applied to the middle electrode, and the TS to the test sample. The TS current will be acquired via the "compensation sample". Using two identical specimens offers the considerable advantage of compensating the polarization and conduction currents which can occur under high fields; the measured current is due solely to the internal field of the thermally excited sample.

The measurement "under applied field" is made in two steps (Fig. 21):

- during the conditioning, the voltage is applied to the middle electrode and the current amplifier is short circuited. Thus, the two samples constitute two identical capacitances placed in parallel with respect to the voltage source (Fig. 21 a).
- in order to prevent the transport of induced charges at the electrodes via the HV generator rather than via the current amplifier, the power source has to be disconnected during the measurement (Fig. 21 b). The TS current is then measured by exciting thermally the studied specimen (in contact with the thermal diffuser), while the current amplifier is connected to the compensation sample. This time, the two samples are in series with respect to the current amplifier, and the short-circuit conditions are fulfilled.

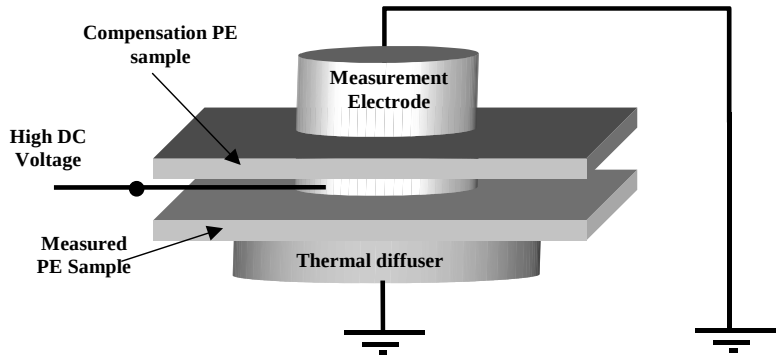

Figure 21a: TSM measurement under applied field: (a) Application of HV.

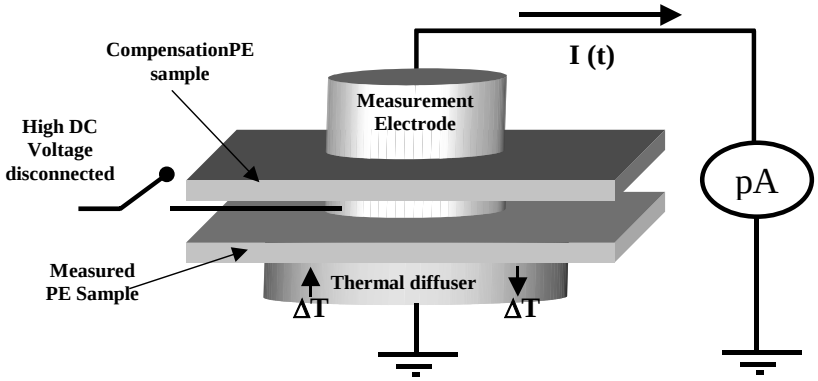

Figure 21b: TSM measurement under applied field: (b) Acquisition of TS current.

The TS current in the external circuit is:

$$I(t) = -\alpha C_2 \int_{x_0}^{x_0+d} E(x) \frac{\partial \Delta T(x,t)}{\partial t} dx \tag{42}$$

where C_2 is the capacitance seen by the current amplifier.

(a) Capacitance seen by the current amplifier

During the measurement, the two samples are in series, and, if they are identical, $C_2 = C/2$. If no voltage is applied to the samples ("voltage off"), the TS current should be half of that given by a measurement made on the thermally excited sample under short-circuit conditions, where $C_2 = C$.

(b) Low fields applied to virgin samples

For low applied fields, when there is no charge injection into the sample and the sample is assumed as virgin, the electric field can be considered as constant throughout the material and identical to the applied field E_e : $E(x) = E_e = V/d$, where V is the applied voltage. In this case, the TS current in Equation (42) becomes directly proportional to the applied voltage:

$$I(t) = -\alpha C_2 \frac{V}{d} \int_{x_0}^{x_0+d} \frac{\partial \Delta T(x,t)}{\partial t} dx \tag{43}$$

This current can be used for calibration purposes and for deconvolution.

(c) Low fields applied to samples containing space charge

If the test sample already contains space charge giving a residual field $E_r(x)$, and an electric field ($E_e = V/d$ which does not modify the space charge distribution) is applied externally, the total field in the sample becomes $E(x) = E_r(x) + E_e$. Equation (42) can then be written as:

$$I(t) = -\alpha C_2 \int_{x_0}^{x_0+d} \left[E_r(x) + E_e \right] \frac{\partial \Delta T(x,t)}{\partial t} dx$$

$$= -\alpha C_2 \int_{x_0}^{x_0+d} E_r(x) \frac{\partial \Delta T(x,t)}{\partial t} dx - \alpha C_2 E_e \int_{x_0}^{x_0+d} \frac{\partial \Delta T(x,t)}{\partial t} dx \tag{44}$$

$$= I_0(t) - \alpha C_2 \frac{V}{d} \int_{x_0}^{x_0+d} \frac{\partial \Delta T(x,t)}{\partial t} dx = I_0(t) + I_f(t) \tag{45}$$

where $I_0(t)$ is the current due to the residual space charge and $I_f(t)$ the current due to the external field. Thus, the total current should be the sum of the "voltage off" and the "voltage on" currents.

5.2 Measurement Results by TSM

In this section, several thermal step measurements under "voltage-off" and "voltage-on" conditions are presented. The test specimens are 1 mm-thick flat samples made of XLPE and provided with vacuum deposited aluminum electrodes, with a diameter of 30 mm. Initially, the specimens were at room temperature. The thermal wave has been supplied by a cold liquid (0°C) circulating in a radiator ("thermal diffuser") in contact with the test sample.

Initially a comparison is made of the thermal step currents obtained on the same sample under short-circuit conditions ("single capacitance" – Fig. 19) and by using the "double capacitor" set up, without applying a voltage (Fig. 20). The test sample had been previously conditioned for 180 minutes at 30 kV/mm, 60°C, while the "compensation sample" contained a very low amount of space charge (virgin sample). It can be seen from Fig. 22 that the amplitude of the thermal step current acquired with the "double capacitor" is divided by a factor of 2 with respect to the short-circuit measurement, as indicated in the previous section.

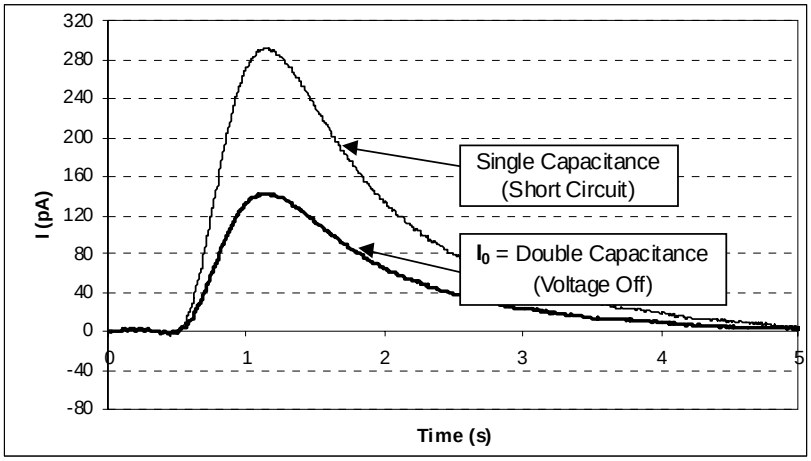

Figure 22: Comparison between the measurements under short-circuit and in "double capacitor".

Fig. 23 shows the thermal step currents obtained "under field" (with the "double capacitor" setup) on a virgin sample. We have first measured the sample without applying any voltage ("voltage off" measurement). A weak thermal step current can be seen. This indicates a small amount of space charge in the bulk of the polyethylene sample due to the manufacturing (as reported in [24]).

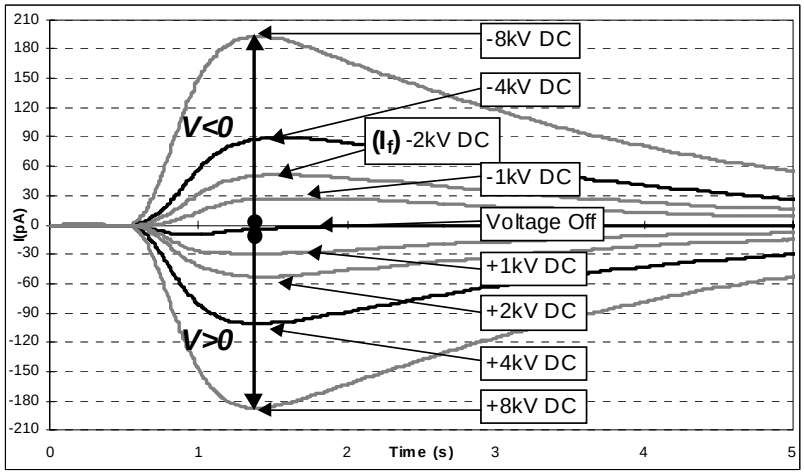

Figure 23: "Under field" TS signals obtained on a flat unconditioned XLPE sample (1 mm-thick) subjected to various dc voltages.

The sample has then been submitted to several positive and negative voltages. Each voltage has been applied for several dozens of seconds, then the power source has been disconnected and the TSM measurement performed. For every voltage, an electrostatic voltmeter verified that the voltage remained constant on the middle electrode during the TSM measurement.

Below 8 kV, the amplitude of the TS signals is multiplied by two each time the applied voltage doubles: the ratio I_{+2kV}/I_{+1kV} is 2, and the ratio I_{+4kV}/I_{+1kV} is nearly 4 (Fig. 23). When the polarity of the applied voltage is reversed, the signs of the signals are also reversed, and the ratios between the TS currents are equal to the ratios between the applied voltages. It can be concluded that the proportionality between the acquired signal and the applied voltage (equation (43)) is verified for low applied fields (≤4 kV/mm).

The fact that low applied external fields do not modify the space charge distribution within the sample, but just add to the remnant electric field is illustrated in Figs. 24 and 25. Actually, Fig. 24 shows that the mean of the thermal step currents I_{+1kV} and I_{-1kV} superposes perfectly to the current I_0 measured in "voltage-off" conditions. The deconvolution presented in Fig. 25a shows that the electric field within the sample placed under -2 kV DC is quasi equal to the field resulting from the "voltage off" TSM measurement increased by 2 kV/mm. In Fig. 25b, it is clear that the space charge distribution within the sample is hardly affected by the application of the external field.

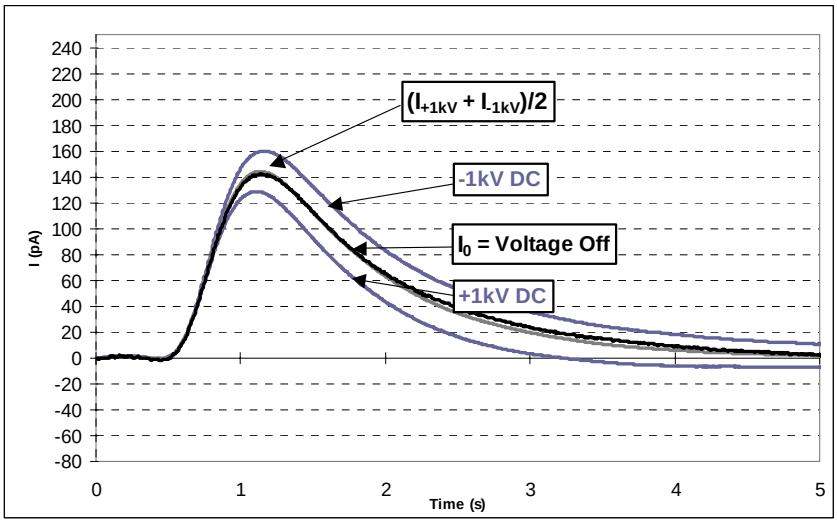

Figure 24: Experimental validation of Equation (43).

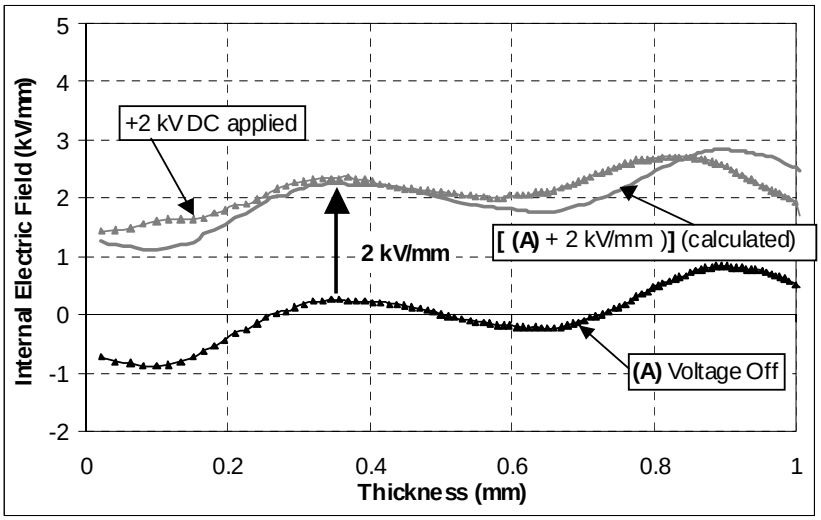

Figure 25a: Validation of Equation (44) on unconditioned sample: residual electric field.

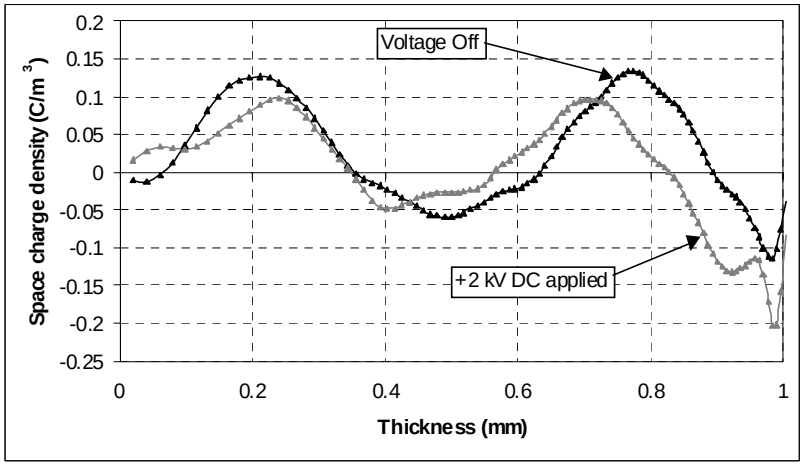

Figure 25b: Validation of Equation (44) on unconditioned sample: space charge

distributions,resulting from “voltage off” and “+2 kV dc” measurements.

When the applied field increases, charge injection in the samples is likely to occur. In this case, the electric field is no longer constant throughout the sample: $E(x) \neq V/d$. The field cannot be inserted before the current integral in Equation (43) and the proportionality between the field and the TS current should no longer be valid. This is well illustrated by the TS measurements made at +8 kV and –8 kV (Fig. 23): the ratios I_{+8kV}/I_{+1kV}.and I_{-8kV}/I_{-1kV} are less than 8. In these cases, the external field has apparently modified the internal space charge distribution.

6. Standard Measurement Conditions for the Thermal Step Method

6.1 Sample Thickness, Amplitude of Thermal Step and acquisition Time

As can be seen from equation (40), the amplitude of the thermal step current depends mainly on four parameters: the thermal constant α, the capacitance of the sample, the remaining electric field and the amplitude of the thermal step. It is then obvious that the thermal step current would be much higher if the capacitance of the sample and the thermal step are large. The combination of these two parameters indicates that the TSM is not really limited by sample thickness, but its sensitivity depends on the sample capacitance and on the ability of the thermal source to transfer the thermal step efficiently to the sample. Thus, the thicker the sample, the more powerful the thermal source. However, care must be taken to avoid temperature elevations which could cause undesired thermally stimulated discharge. The use of a negative thermal steps is preferable because cooling the sample does not affect its charging state (a check is made that no change of phase appears in the thermal step area).

A thermal step of +/- 30 K generated in a light copper radiator with a surface area of 2500 mm² is sufficient to characterize a wide range of insulating samples with thicknesses between 500 nm and 5 mm. For an efficient thermal contact, the sample must be pressed firmly onto the radiator (preferably by a constant pressure system, which ensures good reproducibility). A minimum acquisition time t_a can be roughly estimated with the relation $\boldsymbol{t_a > W(x_0 + d)^2}$, where W is the reciprocal of the thermal diffusivity of the material, d its thickness and x_0 the equivalent-added thickness which takes into account the thermal loss at the radiator/sample interface defined in §5.1. The parameter x_0 can be calculated by calibration and, for a good thermal contact, it is of the order of 1 mm. In practice, the acquisition can be stopped when the value of the TS current approaches zero (this indicates that the temperature within the sample has ceased to vary, $\partial \Delta T / \partial t \rightarrow 0$). For thicknesses between 500nm and 2mm, the acquisition times are in the range of 1s to 20s (the thinner the sample, the smaller the acquisition time). The acquisition times observed in practice are obviously bigger than the estimation t_a.

For most solid insulators, the value of constant α lies between 10^{-6} and 10^{-3} K^{-1}. For any material, the value of α can be determined by calibration, with polar dielectrics having the highest values of α.

6.2 Generation of Thermal Step

There are several ways to generate the thermal step (e.g. by mean of a liquid coolant, an expanding gas or the Joule effect). The simplest way is undoubtedly to flow a liquid through a radiator by computer-controlled hydraulic pumps (Fig. 26). The choice of the liquid is determined by the desired thermal step. Glycol or water-alcohol blends are satisfactory for thermal steps of several dozens of degrees. If a negative thermal step is used, then the reheating of the sample back to the initial temperature can be easily carried out with a warm liquid, and allows the measurement to be repeated.

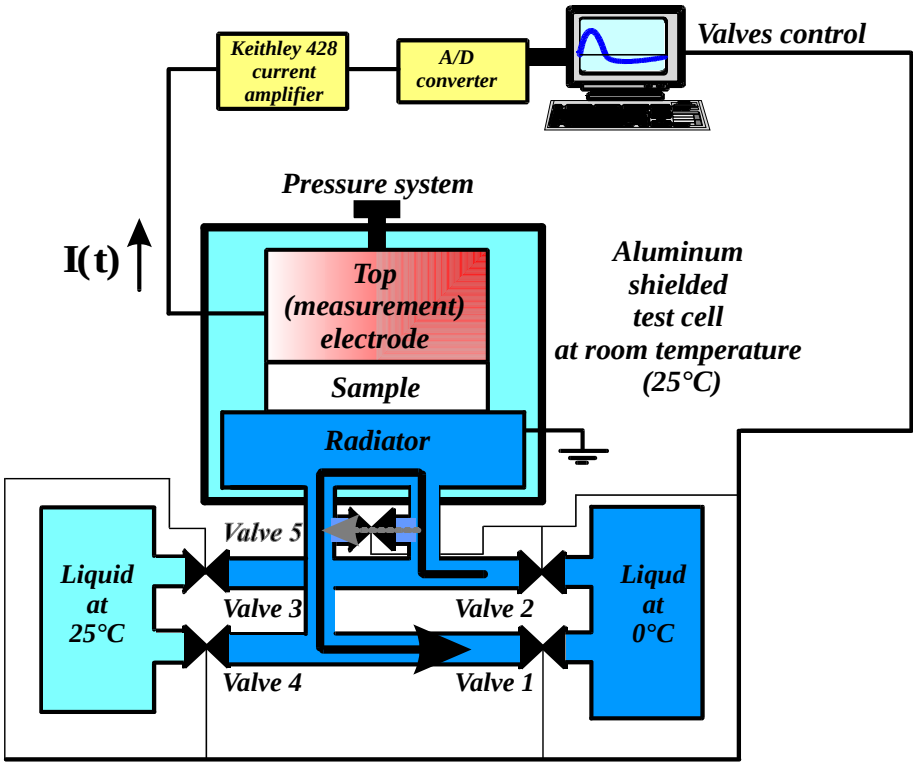

Figure 26: Diagram of the TS setup.

6.3 Measurement of TS current

An instrument able to measure currents of the order of 1 pA within a frequency range of 1 kHz is needed to acquire the TS signals. The sensitivity of most electrometers is lower than 1 pA, but, in turn, their rise time is usually of the order of a second and this makes few of them suitable for TS measurements. Appropriate choices for the TSM are current amplifiers, which provide better dynamic characteristics than electrometers.

6.4 Shielding from Electric Noise

Under laboratory conditions it is possible to make TS measurements without particular shielding, except for the measurement leads. In noisy environments, it is recommended to place the measurement cell (thermal diffuser, sample and measurement electrodes) in a Faraday cage to

reject electromagnetic interference.

7. Calibration and De-convolution for TSM

7.1 Calibration

Consider an insulating sample which contains an amount of space charge inducing a remaining electric field $E_r(x)$. If the sample is subjected, under a "double capacitor" set up, to a low external field $E_e = V/d$ which does not provoke charge injection and does not modify the position of the charge within the sample, the measured TS current, I_+, will have an expression analogous to (44):

$$\boldsymbol{I_+(t) = -\alpha \frac{C}{2} \int_{x_0}^{x_0+d} \left[E_r(x) + E_e\right] \frac{\partial \Delta T(x,t)}{\partial t} dx} \tag{46}$$

The application to the specimen of an external field with the same value as E_e but of opposite polarity will give a thermal step current I_- such as:

$$\boldsymbol{I_-(t) = -\alpha \frac{C}{2} \int_{x_0}^{x_0+d} \left[E_r(x) - E_e\right] \frac{\partial \Delta T(x,t)}{\partial t} dx} \tag{47}$$

The difference between the currents obtained by the two "under field" measurements will then be:

$$\begin{aligned} &\boldsymbol{I_D(t) = I_+(t) - I(t) = -\alpha C \int_{x_0}^{x_0+d} E_e \frac{\partial \Delta T(x,t)}{\partial t} dx = -\alpha C E_e \int_{x_0}^{x_0+d} \frac{\partial \Delta T(x,t)}{\partial t} dx =} \\ &\boldsymbol{-2\alpha \frac{C}{2} E_e \int_{x_0}^{x_0+d} \frac{\partial \Delta T(x,t)}{\partial t} dx = -2\alpha \frac{C}{2} \frac{V}{d} \int_{x_0}^{x_0+d} \frac{\partial \Delta T(x,t)}{\partial t} dx = 2\, I_C(t)} \end{aligned} \tag{48}$$

where $I_C(t)$ is defined as

$$\boldsymbol{I_C(t) = -\alpha \frac{C}{2} \frac{V}{d} \int_{x_0}^{x_0+d} \frac{\partial \Delta T(x,t)}{\partial t} dx} \tag{49}$$

The current $I_C(t)$, which is a function of the applied voltage and the material parameters, is referred to as the **calibration current**. If the measured sample initially contains little space charge (the remaining field is negligible with respect to V/d), then $E(x) = V/d$ and Equation (43) is obtained with $C_2 = C/2$.

By using the calibration current $I_C(t)$, the calibration voltage V, the thickness of the sample d and the parameter α, Equations (48) and (49) allow the calculation of the quantity

$$\boldsymbol{J(t) = \int_{x_0}^{x_0+d} \frac{\partial \Delta T(x,t)}{\partial t} dx = -\frac{I_D(t)}{\alpha C V/d} = -\frac{2\, I_C(t)}{\alpha C V/d}} \tag{50}$$

and then the determination (e.g. by a least-squares fit) of the parameters W and x_0.

7.2 Processing the Thermal Step Current

In the following, it is assumed that there are two TS currents, namely $I_1(t)$ and $I_2(t)$, acquired by applying the thermal step to each of the two sides of a sample submitted to a dc voltage V. The problem is to find the internal electric field $E(x)$ by using this data and a calibration current $I_C(t)$.

(a) Calculation of E(x) using the mean value theorem

Because the temperature derivative $\partial\Delta T(x,t)/\partial t$ has a constant sign at every moment t, and applying the mean value theorem [27] to the expression of the TS current, Equation (40), the following is derived:

$$I(t) = -\alpha C \int_{x_0}^{x_0+d} E(x)\frac{\partial\Delta T(x,\ t)}{\partial t}dx = -\alpha C E(y(t)) \int_{x_0}^{x_0+d} \frac{\partial\Delta T(x,t)}{\partial t}dx \tag{51}$$

where $y(t)$ takes values within the gap $[0,\ d]$ (y takes particular values of x). Therefore, each value taken by $E(y)$ is a value of $E(x)$.

Consider the heat transfer in the sample taking place as in an infinite semi-plane, the function $\partial\Delta T(x,t)/\partial t$ has the expression [28]:

$$\frac{\partial\Delta T(x,t)}{\partial t} = \Delta T \frac{x}{t}\left(\frac{W}{4\pi t}\right)^{\frac{1}{2}} \exp\left[-\frac{W(x)^2}{4t}\right] \tag{52}$$

Naturally, it is assumed that the thermal step ΔT is applied at $x=0$.

Then, from the integral in Equation (51), $J(t)$, becomes:

$$J(t) = \int_{x_0}^{x_0+d} \frac{\partial\Delta T(x,t)}{\partial t}dx = \int_{x_0}^{x_0+d} \Delta T \frac{x}{t}\left(\frac{W}{4\pi t}\right)^{\frac{1}{2}} \exp\left[-\frac{W(x)^2}{4t}\right]dx \tag{53}$$

and gives :

$$J(t) = \Delta T\left(\frac{1}{\pi W t}\right)^{\frac{1}{2}}\left[\exp\left[-\frac{W{x_0}^2}{4t}\right] - \exp\left[-\frac{W(x_0+d)^2}{4t}\right]\right] \tag{54}$$

As shown in Equation (50), the comparison between the calibration current $I_C(t)$ and the factor $-\alpha C E_e J(t)/2$ allows the parameters x_0 and W to be calculated.

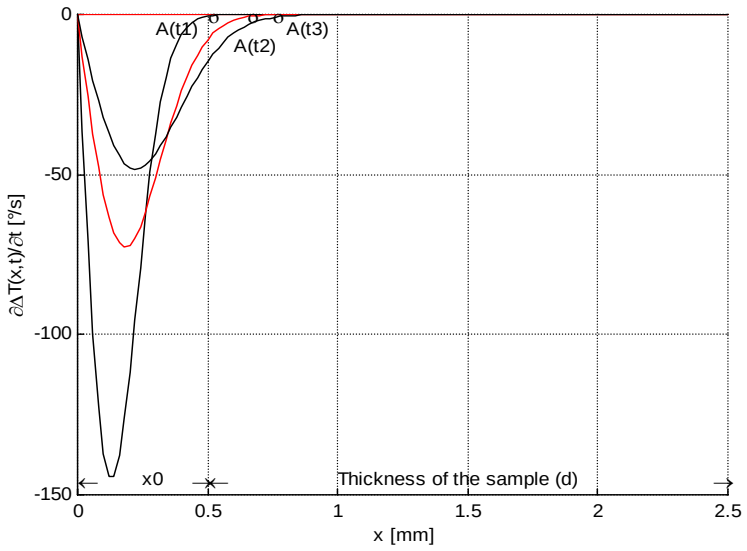

Figure 27: Evolution of "thermal wave" within the sample.

Figure 27

Fig. 27 shows that the temperature derivative, Equation (52), is a decreasing function which has the appearance of a wave. The abscissa $A(t)$ corresponds to the position x where the exponential of the function approaches zero : $A(t)=x$ for $\exp\left[-\frac{Wx^2}{4t}\right]\to 0$. This gives $\boldsymbol{A(t)=Coe\sqrt{t/W}}$, with Coe=3, 4, 5…, with respect to the desired precision. The variable $A(t)$ can be considered as a virtual electrode.

If it is assumed that $y(t)$ varies in a similar manner, $\boldsymbol{y(t)=Coe'\sqrt{t/W}}$, $y(t)$ can be found by using the two measured currents $I_1(t)$ and $I_2(t)$. A first distribution of $E(y)$ is given by $I_1(t)$:

$$\boldsymbol{E_1(y)=E_e\frac{I_1(t)}{I_c(t)}} \tag{55}$$

A second distribution of $E(y)$ is given by using the second current $I_2(t)$:

$$\boldsymbol{E_2(d-y)=-E_e\frac{I_2(t)}{I_c(t)}} \tag{56}$$

In the middle of the sample, $\boldsymbol{E_1(\frac{d}{2})=-E_2\left(\frac{d}{2}\right)}$. This relation allows determining $y(t)$, then the internal field $E(x)$ and the space charge density $\rho(x)=\varepsilon\frac{\partial E(x)}{\partial x}$.

(b) Calculation of E(x) by using the electric potential V(x)

With the heat transfer in the sample occurring as in an infinite semi-plane, $I_C(t)$ can be written as:

$$I_C(t) = E_e \frac{\alpha C \Delta T}{\sqrt{\pi W t}} \left[\exp\left(-\frac{W (x_0)^2}{4t} \right) - \exp\left(-\frac{W(x_0 + d)^2}{4t} \right) \right] \tag{57}$$

This expression presents a maximum ($d>>x_0$) for $t = t_M = W x_0^2/2$, this maximum being $I_{CM}(t) = E_e \frac{\alpha C \Delta T}{\sqrt{\pi W t_M}}$ 0,60 . If E_e, C and ΔT are known quantities, and if W is also known, α and x_0 can be calculated.

Then, the mathematical problem is to find $E(x)$ from the integral:

$$I(t) = -\alpha C \Delta T \int_{x_0}^{x_0+d} E(x) \frac{x}{t} \sqrt{\frac{W}{4\pi t}} \exp\left(-\frac{W (x)^2}{4t} \right) dx \tag{58}$$

The term $\exp\left(-\frac{W x^2}{4t} \right)$ is positive and decreases when x increases; this term can be considered negligible when $x \cong x_0+d$. Then, the second mean value theorem [21] applied to equation (58) leads to:

$$I(t) = -\alpha C \Delta T \exp\left(-\frac{W x_0^2}{4t} \right) \int_{x_0}^{z(t)+x_0} E(x) x dx \tag{59}$$

where z takes values comprised between x_0 and x_0+d. By integrating by parts and by putting $V(z) = -\int_{x_0}^{z(t)+x_0} E(x) dx$, the following is obtained:

$$I(t) = \alpha C \Delta T \exp\left(-\frac{W (x_0)^2}{4t} \right) \left[V(z)(z + x_0) - \int_{x_0}^{z+x_0} V(x) dx \right] \tag{60}$$

$V(z)$ can be calculated if it is assumed that the variation of $z(t)$ is of the form $z(t) \approx \sqrt{\frac{t}{W}}$.

The same calculation as in §7.2.(1) with $I_1(t)$ and $I_2(t)$ is then used. In the middle of the sample, the value of $E(d/2)$ must be identical for $I_1(t)$ and $I_2(t)$. Under short-circuit condition $V(d)=0$, and under applied field V_0, $V(d)=V_0$.

(c) Processing by Successive Differentiations

With the previous model of heat transfer, as the temperature derivative is zero between $A(t)$ and d, the upper limit d of the thermal step current integral can be replaced by $A(t)$:

$$I(t) = -\alpha C \int_{x_0}^{A(t)} E(x) \frac{\partial \Delta T(x,t)}{\partial t} dx \tag{61}$$

and after substituting for the temperature derivative from Equation (52):

$$I(t) = -\alpha C \Delta T \sqrt{\frac{W}{4\pi t}} \frac{1}{t} \int_{x_0}^{A(t)} E(x) x \left[\exp\left(-\frac{W x^2}{4t} \right) \right] dx \tag{62}$$

(when $x \to A(t)$, $\exp\left[-\frac{W x^2}{4t} \right] \to 0$).

The second mean value theorem applied to equation (62) gives:

$$I(t) = -\alpha C \Delta T \sqrt{\frac{W}{4\pi t}} \frac{1}{t} \left[\exp\left(-\frac{W x_0^2}{4t} \right) \right] \int_{x_0}^{B(t)} E(x) x dx, \tag{63}$$

with $x_0 < B(t) < A(t)$. Defining $H(t)$ from equation (63) as:

$$H(t) = -\frac{I(t)}{\alpha C \Delta T} \sqrt{\frac{4\pi(t)^3}{W}} \left[\exp\left(\frac{W x_0^2}{4t} \right) \right], \tag{64}$$

gives:

$$H(t) = \int_{x_0}^{B(t)} E(x) x dx \tag{65}$$

The derivative of H with respect to B is: $\frac{dH}{dB} = B\,E(B) = \frac{dH}{dt}\frac{dt}{dB}$. Assuming $B(t)$ has the form $B(t) = Coe\sqrt{\frac{t}{W}}$, then $\frac{dB}{dt} = \frac{Coe}{2\sqrt{Wt}}$, so:

$$\frac{dH}{dB} = \frac{dH}{dt}\frac{dt}{dB} = \frac{dH}{dt}\frac{2\sqrt{Wt}}{Coe} \tag{66}$$

Therefore:

$$\frac{dH}{dB} = E(B)\, Coe \sqrt{\frac{t}{W}} = \frac{dH}{dt}\frac{2\sqrt{Wt}}{Coe} \tag{67}$$

and :

$$E(B) = \frac{dH}{dt}\frac{2W}{(Coe)^2} \tag{68}$$

This relation allows the variation of the electric field within the sample to be calculated.

8. Round Robin Tests

One of the activities of CIGRE Task Force 15.12.1 was to conduct a round robin test to check the calibration of space charge measuring systems. The objectives of the test were:

- to provide "standard" samples that could be easily prepared at low cost, maintain their charge for long periods, and withstand transportation between laboratories on different continents
- to develop techniques to store the "standard" samples and transport them between laboratories
- to develop a "standard" procedure to carry out the calibration tests
- to measure the amount of charge and its spatial resolution
- to compare the results of space charge measurements using the different methods in the same or different laboratories
- to compare the accuracy of the measurements between laboratories

Insulation samples containing space charge were prepared and circulated to about fifteen laboratories in Asia, Europe and North America, The different laboratories were equipped to perform space charge measurements using one or more of the pressure wave pulse (PWP), pulse

electroacoustic (PEA) or thermal step methods. The samples chosen were corona charged polyethylene terephthalate (PET) on the basis that they were easier to prepare than electron irradiated samples. The results of the tests from about twelve laboratories were not consistent either within or between laboratories. Some laboratories measured small amounts of space charge in some samples and no charge in others. The main reason was the inconsistency in the samples. As a result it was decided that corona charged samples were not suitable for calibration purposes. There was considerable discussion as to the use of either electron irradiated specimens or to use a sample with two internal electrodes that did not affect the acoustic properties of the sample and to which a known voltage could be applied [29]. A decision on the type of sample has not yet been made and no further tests have been carried out.

9. Conclusions

This report is the result of work performed under CIGRE Working Group D1.12 (Materials for DC Applications), Task Force 1 in the period of 2000 to 2003. The guide for space charge measurements in dielectrics and insulating materials gives a description of the physical background of the methods for space charge measurements and discusses the most important aspects concerning the use of the different methods. The dependency of the performance of the methods on parameters such as, for example, the applied electrical, acoustical or thermal pulse is covered in detail. Proper control of these parameters is, together with the correct calibration of the measuring system, essential for reliable and repeatable measurements.

The guide describes the following, widely used pressure and thermal step methods:

- Piezoelectric Induced Pressure Wave Propagation (PIPWP),
- Laser Induced Pressure Propagation (LIPP),
- Pulsed Electro-Acoustic Method (PEA), and the
- Thermal Step Method (TSM)

There is a thorough description of the measuring methods. The role of several parameters is described such as sample thickness and pulse width vs. spatial resolution and transducer thickness. Methods of matching the acoustic impedance of the electrode material are included to obtain the optimum test configuration and also for generating a nanosecond HV pulse or a nanosecond pressure pulse.

For the thermal step method (TSM) the main measuring principle is given together with examples under short circuit conditions and under applied DC Voltage. The influence of important parameters is shown, such as:

- Sample thickness
- Amplitude of the thermal step
- Acquisition time

Methods for the thermal step generation and current measurement are described, followed by a thorough treatment of how to analyse and process the measured thermal step current.

For all the methods the role of the signal detecting circuit is treated in the report. Other aspects covered are shielding of electrical noise and deconvolution for compensation of signal distortion from the measuring system. The necessity of proper calibration for reliable testing is emphasized and the main principles are described. Finally, references are given for further reading on the origin and application of these methods for space charge measurements in dielectrics.

10. References

[1] J. Densley, et al, “Space Charge Measurements Techniques: A Review”, *Electra*, TF-15.00.03, No.187, pp.75-89, December 1999.

[2] W. Eisenmenger and M. Haardt: "Observation of Charge Compensated Polarization Zones in Polyvinyliden-fluoride (PVDF) Films by Piezo-electric Acoustic Step Wave Response", *Solid State Commun.*, Vol. 41, pp. 917-920, 1982.

[3] G.M. Sessler, J.E. West, R. Gerhard-Multhaupt and H. von Seggern, “Nondestructive Laser Method for Measuring Space Charge Profiles in Irradiated Polymer Films”, *IEEE Trans. Nucl. Sci.*, Vol. 29, pp. 1644-1649, 1982.

[4] C. Alquie, G. Dreyfus and J. Lewiner, “Stress Wave Probing of Electric Field Distribution in Dielectrics”, *Phys. Rev. Lett.,* Vol. 47, pp. 1483-1487, 1981.

[5] T. Takada, T. Maeno and H. Kushibe: "An Electric Stress-pulse Technique for the Measurement of Charges in a Plastic Plate Irradiated by Electron Beam", *IEEE Trans. On EI,* Vol. EI-22, pp. 497-501, 1987.

[6] Ying Li, M. Yasuda and T. Takada: "Pulsed Electro-acoustic Method for Measurement of Charge Accumulation in Solid Dielectrics", *IEEE Trans. on DEI,* Vol. 1, No. 2, pp. 188-195, 1994.

[7] Y. Li, T. Takada, H. Miyata and T. Niwa, "Observation of Charge Behavior in Multiply Low Density Polyethylene", *J. Appl. Phys.,* Vol. 74, No. 4, pp. 2725-2730, 1993.

[8] X. Qin, K. Suzuki, Y. Tanaka and T. Takada, “Three-dimensional Space Charge Measurement in a Dielectric using the Acoustic Lens and PWP Method”, *J. Phys. D: Appl. Phys,* Vol. 32, pp. 156-160, 1999.

[9] K. Murata, Y. Tanaka and T. Takada, “Space Charge Formation in Cross-linked Polyethylene under AC Voltage”, *Trans. IEE Japan,* Vol. 116-A, No. 12, pp. 1095-1000, 1996.

[10] M. Kojima, Y. Tanaka, T. Takada, and Y. Ohki, “Measurement of Space Charge Accumulation in Gamma-irradiated Polyethylene with DC Voltage”, *Trans. IEE Japan,* Vol. 115-A, No.2, pp. 93-98, 1995.

[11] J.M. Fourmigue, C. Alquie and J. Berdala, “Material Anisotropy Effects on Space Charge Distribution in High Voltage Cable”, *Proc. of IEEE 8th ISE (Paris)*, pp. 922-927, 1994.

[12] N. Hozumi, H. Suzuki, T. Okamoto, K. Wakanabe and A. Watanabe, "Direct Observation of Time-dependent Space Charge Profiles in XLPE Cable under High Electric Field", *IEEE Trans. on DEI,* Vol. 1, No. 6, pp. 1068-1076, 1994.

[13] A. Cherifi, M. Abou Dakka and A. Toureille, "The Validation of the Thermal Step Method", *IEEE Trans. on EI,* Vol. 27, No. 6, pp. 1152-1158, 1992.

[14] M. Abou-Dakka, S.S. Bamji and A.T. Bulinski, "Space Charge Distribution in XLPE, by TSM, using the Inverse Matrix Technique", *IEEE Trans. on DEI,* Vol. 4, No. 3, pp. 314-320, 1997.

[15] P. Notingher, S. Agnel and A. Toureille, "Thermal Step Method for Space Charge Measurements under Applied DC Field", *IEEE Trans. on DEI,* Vol. 8, No. 6, pp. 985-994, 2001.

[16] A. Toureille, P. Notingher jr, N. Vella, S. Malrieu, J. Castellon and S. Agnel, “The Thermal

Step Technique: an Advanced Method for Studying the Properties and Testing the Quality of Polymers", *Polymer International,* Vol. 46, No. 2, pp. 81-92, 1998.

[17] G. Platbrood, G. Geerts, S. Agnel, N. Vella and A. Toureille, "Study of Direct Current Charging Ability of High Voltage XLPE Cable", *Revue de l'Electricité et de l'Electronique, Special Issue : Câbles d'énergie et science des isolants,* Vol. 3, pp. 57-65, 1998.

[18] S. Agnel, P. Notingher jr., A. Toureille, J. Castellon and S. Malrieu, "Study of Space Charge Dynamics Directly on Power Cables using the Thermal Step Method", *IEEE 1999 CEIDP Annual Report,* pp. 50-53, 1999.

[19] S. Agnel, A. Toureille and C. Le Gressus, "Study of the Aging of Impregnated Paper of High Power Capacitors using the Thermal Step Method and the Thermally Stimulated Currents", *IEEE 1996 CEIDP Annual Report*, pp. 190-193, 1996.

[20] S. Malrieu, P. Notingher jr, F. Pacreau and A. Toureille, "Influence of Space Charge on Breakdown of Multilayer Epoxy. A Study by the Thermal Step Method", *IEEE 1997 CEIDP Annual Report,* pp. 87-91, 1997.

[21] J. Castellon and A. Toureille " Space Charge Measurement Applied to the Ageing of Industrial Insulating Composite Materials" *CSC'3, Troisième conférence internationale sur la Charge Electrique des Isolants Solides,* Tours, France, pp. 679-683, 1998.

[22] T. Takada, Y. Tanaka, N. Adachi and Xiaoku Qin, "Comparison between the PEA Method and the PWP Method for Space Charge Measurement in Solid Dielectrics", *IEEE Trans. DEI,* Vol. 5, No. 6, pp. 944-951, 1998.

[23] R.E. Collins, "Measurement of Charge Distribution in Electrets", *Rev. Sci. Instrum.,* Vol. 48, pp. 83-91, 1977.

[24] D.K. Dus-Gupta and J.S. Hornsby, "Laser Intensity Modulation Method (LIMM). An Analytical and Numerical Modulation", *IEEE Trans. on EI,* Vol. 26, pp. 63-68, 1991.

[25] D.W.Tong, "Electron Beam Probing of Space Charge in PET Films", *IEEE Trans. on EI,* Vol. EI-17, pp. 377-385, 1982.

[26] A.Toureille, J.P. Reboul and P. Merle, "Détermination des densités de charges d'espace dans les isolants solides par la méthode de l'onde thermique", *Journal de Physique III*, Vol. 1, pp. 111-123, 1991.

[27] A. Doneddu, *Nouveau cours de mathématiques,* 2nd edition, Tome 4, Vuibert Publishing House, Paris, France, 1979.

[28] J.F. Sacadura, *Initiation au transfert thermique*, "Technique et documentation" Publishing House, Paris, France, 1978.

[29] J.T. Holbøll, M. Henriksen and C. Rasmussen, "Dielectric sample with two-layer charge distribution for space charge calibration purposes", *2002 CEIDP*, pp. 648-651, 2002.

Annex A: Simulation results of acoustic multi-reflections in double layer solid dielectrics using acoustic probing measurement of space charge.

In the PEA method, a pulsed electric field is applied to a specimen to generate an acoustic wave the amplitude of which is proportional to the space charge profile. The acoustic wave is detected by a piezoelectric sensor in the PEA system. The space charge profile can be reproduced by the detected acoustic wave profile. However, when a specimen has different acoustic properties from those of the upper electrode and/or a specimen consists of multi-layers, the detected acoustic wave contains signals that are not due to space charges. The acoustic signals generated by the difference in acoustic properties can cause misinterpretation of the space charge measurement. This problem has been investigated using the theoretical equations of transmission and reflection. This approach, however, did not succeed in clarifying the spatial and transient acoustic phenomena. A new numerical analysis model has been proposed to discuss the charge profile observed in multi-layer dielectric materials.

Figure A1(a) shows the composition of the PET/Glass two-layer specimen used in this investigation. The acoustic impedance of the samples and electrode materials are shown in Table A1. The thickness of the PET and glass are 0.19 and 1 mm, and the permittivities of PET and glass are 2.3 and 7.5, respectively. In order to discuss the signals in the sample, a numerical analysis model was used [A1].

Figure A1(d) shows the generation and propagation of acoustic waves obtained from a simulation. Figs.A1(b) and A1(c) show the pulse voltage wave and the sensor output signals of the pressure distribution in the specimen. The vertical and horizontal axes are the time and location. The amplitude in Fig. A1(d) is described by the color shading, with positive in red, and negative in blue. In Fig. A1(d), the sensor is located at x=0.2 mm. The acoustic wave generated at t=0, appearing at the top in the figure, propagates with time, as described towards the bottom. It is clear that the sensor signal at position 0.27μs in Fig. A1(c) is formed by the acoustic wave reflections at the interfaces between the PET and the glass. The acoustic signals in the space charge profile of the PET/glass are not due to space charges and are irrelevant. The signal amplitude in Fig.A1(c) at 0.36μs is attenuated by the superimposition of the negative acoustic wave generated at the glass/upper electrode interface and the positive acoustic wave generated at the PET/glass interface. It proves that the polarity and amplitude of the acoustic wave profiles are affected by these reflections. Figure A1(e) shows the reproduced space charge distribution from the simulation results.

This numerical analysis reveals that the acoustic property of each material should be of concern in space charge measurement of multi-layer samples.

Table.A1. Acoustic Impedance of Specimen and Electrodes

Materials	Acoustic Impedance: Z [kg/m^2/s]	Density: ρ [kg/m^3]	Sound Velocity: c [m/s]
Slide Glass	14×10^6	2470	5669
Semi-con	3×10^6	1500	2000
PET	2.8×10^6	1302	2150
Al-electrode	15×10^6	2500	6000

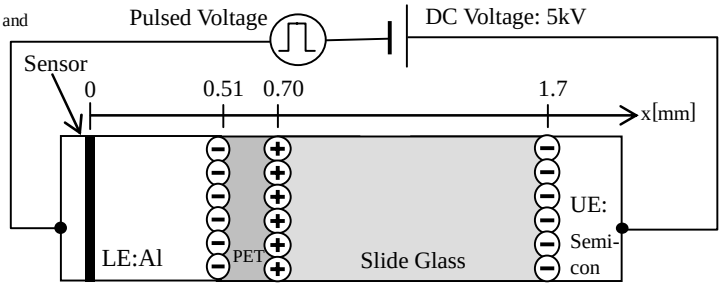

(a) Composition of Samples and Electrodes.

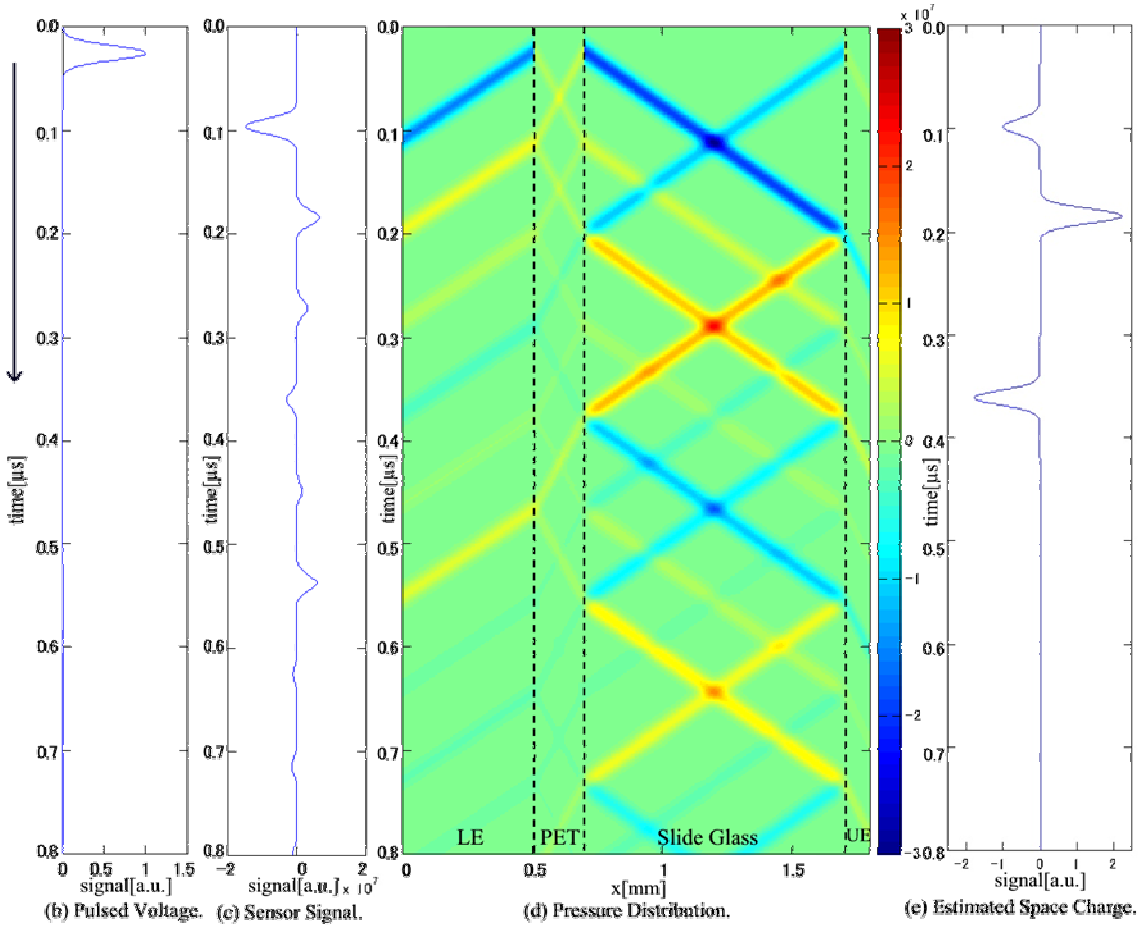

(b) Pulsed Voltage. (c) Sensor Signal. (d) Pressure Distribution. (e) Estimated Space Charge.

[A1] M.Wadamori, M. Fukuma, T. Maeno, K. Fukunaga and M. Nagao, “Proposal of Numerical Analysis Model of Acoustic Wave Propagation and Generation on PEA Method”, Proc. ICPADM(2003), pp.863-866, 2003.